

TUTORIAL | MAY 03 2021

Characterizing polymer structure with small-angle neutron scattering: A Tutorial

Special Collection: [Advances in Processing and Structural Characterization of Complex Soft Matter](#)

Yuan Wei; Michael J. A. Hore  

 Check for updates

J. Appl. Phys. 129, 171101 (2021)
<https://doi.org/10.1063/5.0045841>



Articles You May Be Interested In

A tutorial on the Bayesian statistical approach to inverse problems

APL Mach. Learn. (November 2023)

Tutorial: Simulating modern magnetic material systems in mumax3

J. Appl. Phys. (November 2023)

Tutorial: Thermomechanical constitutive modeling of shape memory polymers

J. Appl. Phys. (March 2022)

02 March 2025 18:16:14

Nanotechnology & Materials Science

Optics & Photonics

Impedance Analysis

Scanning Probe Microscopy

Sensors

Failure Analysis & Semiconductors



Unlock the Full Spectrum.
From DC to 8.5 GHz.
Your Application. Measured.

[Find out more](#)



Characterizing polymer structure with small-angle neutron scattering: A Tutorial

Cite as: J. Appl. Phys. **129**, 171101 (2021); doi: [10.1063/5.0045841](https://doi.org/10.1063/5.0045841)

Submitted: 29 January 2021 · Accepted: 10 April 2021 ·

Published Online: 3 May 2021 · Corrected: 7 May 2021



View Online



Export Citation



CrossMark

Yuan Wei and Michael J. A. Hore^{a)} 

AFFILIATIONS

Department of Macromolecular Science and Engineering, Case Western Reserve University, 10900 Euclid Avenue, Cleveland, Ohio 44106, USA

^{a)}Author to whom correspondence should be addressed: hore@case.edu

ABSTRACT

Small-angle neutron scattering (SANS) is a powerful technique that has been widely used to study polymer materials. In particular, it can provide information on the size, shape, and structure of polymers as well as associated thermodynamic quantities. However, to properly design SANS experiments and correctly interpret the results, it is necessary to understand the unique advantages inherent to neutron scattering measurements of soft materials and the underlying principles of the technique. In addition, it may be necessary to construct new scattering models. In this Tutorial, we provide an overview of SANS and a guide to interpreting SANS measurements of polymers that is aimed at new and prospective users—focusing on standard plots, models, and simple methods by which new models can be quickly constructed.

Published under an exclusive license by AIP Publishing. <https://doi.org/10.1063/5.0045841>

I. INTRODUCTION

Polymers and polymer composites are widely used materials that have received significant attention across the past several decades.^{1,2} Key concepts that are critical to understanding their behavior include the size, conformation, and relaxation dynamics of the chains that comprise the material and how those quantities vary in response to the assembly of the polymers or their response to external stimuli. Stimuli-responsive “smart” polymers^{3,4} can respond in a reversible way to external stimuli, such as temperature or pH, and have garnered interest for medical and drug delivery applications. When used in applications such as thermoresponsive membranes, the selection quality, pore size, and permeability of the materials can be modulated by varying the temperature near the polymer’s lower critical solution temperature (LCST).^{5–7} For such polymers, a coil-to-globule transition is triggered when the LCST is crossed, resulting in a more compact conformation of the chains.

Individual polymer chains themselves can occur as many different architectures, including as linear chains, star-branched or dendritic chains, bottle brushes, rings, and so on.⁸ In solution, the chains may be ideal, swollen, or collapsed and, as noted above, may change their conformation in response to changes in temperature, etc.⁹ The different architectures can influence many polymer

properties, such as their conformation, critical temperatures, and mechanical properties. For example, it is known that cyclic (i.e., ring) polymers do not experience entanglements whereas linear polymers do. Similarly, architectural differences between mostly linear high density polyethylene (HDPE) and branched low density polyethylene (LDPE) affects the degree to which HDPE and LDPE crystallize and subsequently the mechanical properties of polyethylene materials.¹⁰ More specifically, LDPE materials display lower tensile strength and rigidity and increased ductility, as compared to HDPE materials.¹¹ In terms of responsive polymers, the LCST of star-branched poly(*N*-isopropylacrylamide) (PNIPAM) was found to decrease as the number of arms increased and was lower compared to linear PNIPAM.¹² For star polymers with a large number of arms f , the conformation of the arms may be stretched relative to that of linear chains or star polymers with low values of f .^{13,14}

Copolymers combine multiple, chemically distinct monomers into a single chain. Block copolymers¹⁵ that incorporate hydrophilic and hydrophobic blocks are also promising materials for producing intricate ordered structures, such as flower-like or corona-like micelles in solution.^{3,16,17} Moreover, as block copolymers self-assemble, they may express different phase transition temperatures as a result of either their chemical composition or

02 March 2025 18:16:14

assembled structure (or both).^{17–19} In many cases, to fully characterize the structure of these self-assembled objects and constituent chains, it may not be possible to resort to microscopy techniques. However, due to their size ($\approx 10\text{--}100\text{ nm}$), small-angle scattering with light, x rays, or neutrons is typically ideal for characterizing the relative size and conformation of each distinct component. To effectively accomplish this, it is necessary to develop appropriate models of the scattering intensity (i.e., form factors and structure factors).

Finally, polymer brushes²⁰ are another technologically relevant area in which scattering methods have elucidated our understanding of the underlying physics. Polymers are typically grafted to nanoparticles to enhance their dispersion within solvents or polymer matrices,²¹ and knowledge of the structure of the grafted chains has improved our understanding of how they improve the mechanical, electrical, photonic, and thermal properties of the resulting nanocomposite materials. More recently, we have shown that scattering measurements of brushes on nanoparticle surfaces may produce thermodynamic quantities useful in predicting the behavior of microgels in solution and vice versa.²² In some cases, these quantities may be difficult to obtain through other methods.

In this Tutorial, we will discuss the application of scattering techniques to characterize the size and conformation of polymer chains, including model-independent analysis, choosing a correct scattering model, and the fundamentals of deriving new scattering models in several limiting conditions. Although, strictly speaking, these approaches are applicable to x-ray and light scattering measurements, we restrict our focus to small-angle neutron scattering (SANS) measurements since they provide unique opportunities for detailed explorations of structure through selective deuteration and/or contrast-matching. In addition, this Tutorial considers only elastic neutron scattering. Inelastic and quasi-elastic (QENS) scattering measurements provide information on polymer dynamics and have been described elsewhere.²³ In Sec. II, we briefly introduce fundamental terms and concepts that are necessary for SANS. Section III discusses the use of model-independent functions and “standard plots” that can provide guidance for selecting an appropriate scattering model for data analysis followed by discussion of scattering from different polymer architectures in Secs. IV–VI. In Sec. VII, we describe new developments in analyzing scattering measurements of polymer micelles and polymer-grafted, spherical nanoparticles—including construction of new scattering models. In Sec. VIII, we introduce some more advanced approaches including a brief introduction to using the random phase approximation (RPA) to study polymer thermodynamics with SANS as well as using zero average contrast (ZAC) conditions to extract single-chain information from polymer assemblies and aggregates in solution. We conclude with a brief discussion of evaluating the quality of a fit to a SANS measurement. Although the scope of this Tutorial is directed toward new users of SANS, more advanced texts²⁴ and Hammouda’s comprehensive The SANS Toolbox²⁵ are available for the interested reader. In addition, although it is an important technique for studying soft matter systems, we omit the topic of rheological SANS (Rheo-SANS).²⁶

II. FUNDAMENTAL CONCEPTS

A. Considerations for scattering measurements

Neutrons are subatomic particles composed of one up quark and two down quarks. This combination gives the neutron no net electrical charge and $1/2$ spin, which renders the neutron as a highly penetrating form of radiation and also suitable for scattering measurements of magnetic materials. One primary difference between neutron and x-ray scattering processes is that neutrons scatter mostly from atomic nuclei, while x rays scatter via electromagnetic interactions with the electron cloud. For this reason, neutrons are sensitive to different isotopes that may be present in a sample. In terms of probing polymeric materials, this isotopic sensitivity allows for the selective enhancement of the scattering from a particular component by replacing hydrogen atoms in that region with deuterium atoms. This “contrast variation” approach represents one advantage neutron measurements possess over those using x rays for measurements of polymers. However, neutron sources have the disadvantage of much lower flux as compared to x-ray sources. As an illustrative example, the difference between x-ray and neutron interactions with a material can be appreciated qualitatively in the images of the camera shown in Fig. 1.²⁷ In these images, the transmission of x rays (left) or neutrons (right) is attenuated by the camera due to interactions between its atoms and the incident probing particles. In the image of the camera on the left, x rays are attenuated more strongly by high atomic number elements as seen in the opaque (white) regions. Low atomic number elements allow a larger number of x rays to pass through as seen in the gray regions. In contrast, neutrons are not attenuated solely on the basis of atomic number, and interactions between the neutrons and the nuclei in the sample play a primary role in the resulting transmission. As shown in the image of the camera on the right, regions that strongly attenuate x rays appear more transparent to the neutrons, while other regions (e.g., in the top portion of the camera) become largely opaque to the neutrons. In SANS measurements, a similar effect exists wherein scattering depends strongly on the isotopes present in the sample, which is in contrast to small-angle x-ray scattering (SAXS) measurements that depend on the nature of the electron density in the sample (i.e., the elemental composition).



FIG. 1. Differences in attenuation between (right) neutrons and (left) x rays. The x-ray transmission image of the camera shows attenuation of the incident radiation on the basis of the electron density in different regions of the object. In contrast, the neutrons are attenuated due to interactions between the particles and the various nuclei in different regions of the sample. For this reason, x rays and neutrons “see” differently. Reproduced with permission from E. H. Lehmann and W. Wagner, *Appl. Phys. A* **99**, 627–634 (2010). Copyright 2010 Springer Nature.

02 March 2025 18:16:14

Neutrons can be produced via nuclear fission at reactor sources or by collisions of protons with high atomic number targets at spallation sources. Each production method has its advantages and relative drawbacks, and the two approaches complement one another. The neutrons that are produced can be characterized by their energies according to

$$E = \frac{1}{2} m_n v_n^2 = \frac{h^2}{2m_n \lambda_n^2}, \quad (1)$$

where h is Planck's constant, E is the neutron energy, m_n is the neutron mass, λ_n is the neutron wavelength, and v_n is the neutron speed. Thus, specific values of λ_n can be selected from a chromatic beam by selecting for a particular value of v_n , while the neutron energy can be adjusted by passing the particles through a liquid hydrogen or a deuterium cold source to obtain particles with energies in the milli-electronvolt (meV) range.^{28,29}

Neutron scattering occurs due to interactions between incident neutrons and nuclei within the material. The neutron-nucleus interaction potential $V(r)$ can be expressed by the Fermi pseudopotential,^{28,30}

$$V(r) = \frac{h}{m_n} b_i \delta(r), \quad (2)$$

where r is the distance from the scattering center, $\delta(r)$ is the Dirac delta function, and b_i is the neutron scattering length, which characterizes the neutron interaction. Different isotopes yield different values of b_i because isotopes have different nuclear spin states, meaning that neutrons are isotopically sensitive, as previously discussed. The variation of the coherent scattering lengths of various elements for x rays and neutrons is illustrated in Fig. 2. In small-angle scattering, the presence of different elements within a given molecule is captured by the sum of the coherent scattering length of each atom.³¹ For a given substance with a molecular volume v_m containing distinct chemical elements i , the scattering length density (SLD) is defined as

$$\rho = \frac{1}{v_m} \sum_i n_i b_i, \quad (3)$$

where n_i is the number of atoms of i per molecule.²⁹ As an example, for neutrons, this expression yields a value of

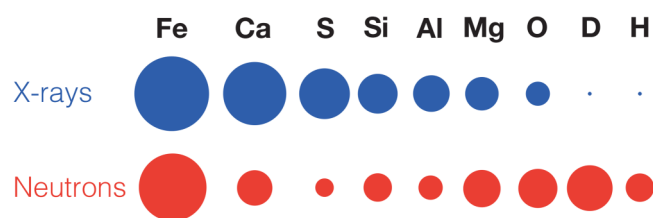


FIG. 2. Schematic of x-ray (top) and neutron (bottom) coherent scattering lengths. The scattering lengths of D and H are identical for x rays but not for neutrons.

$\rho = (30 \text{ \AA}^3)^{-1} (2 \times 6.67 \text{ fm} + 5.80 \text{ fm}) = 6.38 \times 10^{-6} \text{ \AA}^{-2}$ for the SLD of D₂O. The SLD provides the average scattering length over the volume of a molecule instead of a single atom. As discussed below, the scattering signal from a polymer is proportional to $\Delta\rho^2 = (\rho_p - \rho_s)^2$, where the indices p and s correspond to the polymer and solvent, respectively. Since the SLD depends on the isotopes present, it is possible to blend hydrogenated and deuterated solvents together to modulate the SLD of the solvent as $\rho_s = \phi_H \rho_{s,H} + (1 - \phi_H) \rho_{s,D}$, where ϕ_H is the molar fraction of the hydrogenated component. Clearly, if $\rho_s = \rho_p$, the scattering signal from the polymer will vanish. On one hand, this implies that for optimal scattering measurements, the “contrast” $\Delta\rho$ between the components should be maximized by a suitable choice of isotopes in the polymer and solvent/matrix components. For x-ray measurements, in particular, because the contrast depends primarily on differences in the electron density of the molecules, it can be difficult to obtain sufficient contrast between the polymer and its environment. On the other hand, this also implies that “contrast-matching” between components, wherein the SLD of one component is made equal to that of the solvent/matrix, may be used to isolate scattering from only one component of interest when probing multicomponent systems.^{32–35} In choosing appropriate deuteration schemes for SANS measurements, it is also important to realize that the background in the measurement, due primarily to the presence of hydrogen in the sample, acts as noise and may obscure features of the scattering measurements. Therefore, for SANS and other techniques that depend on the coherent scattering signal (e.g., reflectometry and neutron spin echo spectroscopy), one should aim to reduce the amount of hydrogen in the sample; in practice, this typically means reducing the amount of hydrogen in the solvent/matrix component if at all possible. Although incoherent scattering from hydrogen and other elements contributes significantly to the background in a scattering measurement, there are other contributions as well such as electronic noise in the detector or neutrons from other sources.²⁴ For this reason, the background must be measured and cannot be calculated solely from the incoherent scattering anticipated for a particular sample on the basis of its composition.

B. Small-angle neutron scattering (SANS)

SANS is an elastic scattering technique, meaning that for a neutron with momentum $\mathbf{p} = \hbar\mathbf{k}$, the magnitudes of the initial and final wave vectors are equal, i.e., $|\mathbf{k}_f| - |\mathbf{k}_i| = 0$, no energy is transferred, and only the direction of the neutron changes. Inelastic scattering occurs when there is a transfer of both momentum and energy, while quasi-elastic scattering is a form of inelastic scattering where the energy transfer peak is located near zero. Quasi-elastic neutron scattering is often referred to as QENS. Inelastic and quasi-elastic scattering techniques are used to probe dynamics in systems,^{23,36,37} while elastic scattering provides structural and thermodynamic information.²⁴ In both classes of techniques, information at different length scales is obtained by observing scattering intensities at different values of the scattering angle.

The scattering angle is characterized by $\mathbf{Q} = \mathbf{k}_f - \mathbf{k}_i$, which is referred to by several names including the scattering vector, momentum transfer, or the scattering variable. Under the elastic scattering condition, $Q = |\mathbf{Q}|$ can be defined²⁹ from \mathbf{k}_f and \mathbf{k}_i , as

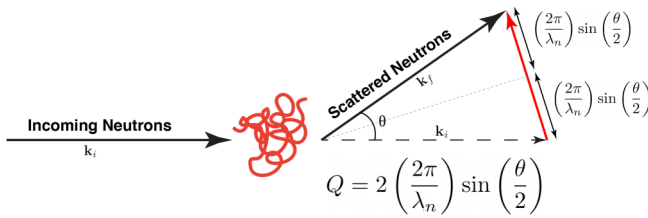


FIG. 3. The scattering vector Q (red arrow) as defined in terms of the momentum (solid black arrows) of the incoming and scattered neutrons. The initial and final wave vectors corresponding to these momenta, \mathbf{k}_i and \mathbf{k}_f , respectively, are shown beneath the incoming and scattered vectors. The dashed arrow represents the incoming vector, translated to coincide with the scattered vector.

illustrated in Fig. 3, as

$$Q = 2|\mathbf{k}| \sin\left(\frac{\theta}{2}\right) = \left(\frac{4\pi}{\lambda_n}\right) \sin\left(\frac{\theta}{2}\right). \quad (4)$$

Since Q is a coordinate in a reciprocal space, large values of Q correspond to large angles and probe structure at small length scales. Conversely, small values of Q (the “low- Q ” region) probe structure at larger length scales.³⁶ In practice, typical values of λ_n at cold neutron facilities fall between approximately 5 and 10 Å.

The measured scattered neutron signal corresponds to the macroscopic differential scattering cross section and includes a Q -dependent, coherent term and a Q -independent, incoherent background. After reduction of scattering data, which accounts for the details of the experimental instrumentation, the measured scattering intensities $I(\theta, \lambda_n) \rightarrow I(Q)$,²⁴ and

$$I(Q) = \frac{d\Sigma_{coh}(Q)}{d\Omega} + \frac{d\Sigma_{inc}}{d\Omega}. \quad (5)$$

It is common for SANS intensities to be expressed in absolute intensities with units of cm^{-1} , which, in principle, should be independent of the instrument used for the measurement.¹⁰ For a binary system containing two components, such as a polymer in solution, $I(Q)$ depends only on the contrast between the components, a constant background B that contains incoherent contributions, and the form factor of the component of interest (e.g., component 1),¹⁰

$$I(Q) = \phi_1(\Delta\rho)^2 V_1^2 P_1(Q) S_I(Q) + B, \quad (6)$$

where ϕ_1 is the number density of component 1, V_1 is the volume of a single particle of component 1, and the contrast between the SLDs of the two components is expressed as $\Delta\rho = (\rho_1 - \rho_2)$. Note that if an appropriate blank sample is measured, it is possible to subtract the background such that in Eq. (6), $B = 0$. $S_I(Q)$ is the inter-particle structure factor and represents correlations between the positions of the scattering particles within the sample. Under dilute conditions, these positions are not correlated and $S_I(Q) \approx 1$, which is an approximation we will make throughout the remainder of this Tutorial. At higher concentrations, where

$S_I(Q) \neq 1$, a suitable function can be included by considering how the particles might interact and solving the Ornstein-Zernike equation.^{24,25} Commonly used structure factors are included as a part of many software packages such as SasView, and the selection of the appropriate function will vary depending on the details of the system. In the dilute solution limit, the task of analyzing SANS measurements reduces to choosing (or deriving) an appropriate model of the particle’s form factor $P(Q)$. As will be demonstrated in Secs. III–VIII, $P(Q)$ can be expressed in terms of the form factors, $P_i(Q)$, and form factor amplitudes, $F_i(Q)$, of the various components that comprise the particle/molecule of interest.^{10,24}

C. Scattering and the Fourier transform

The form factor and the form factor amplitude describe the structure of a particle as seen by scattering measurements. The origin of these terms can be understood by writing the wave that describes the incident neutrons as a plane wave,

$$\psi_i(\mathbf{r}, t) = A \exp[-i(\omega t - \mathbf{k}_i \cdot \mathbf{r})]. \quad (7)$$

The plane wave will scatter from all nuclei that are within the object of interest, and each scattering event will produce an outgoing, scattered wave. The intensity measured for each value of Q will depend on whether or not the interference between the scattered waves is constructive.²⁴ For each nucleus j in the sample, the scattered wave will travel a longer path than the incident wave such that a phase difference of $\mathbf{r}_j \cdot (\mathbf{k}_f - \mathbf{k}_i) = \mathbf{r}_j \cdot \mathbf{Q}$ is introduced, which is the origin of constructive or destructive interference.^{24,38} The average effect of the phase differences can be written as a superposition of the scattering from each nucleus j as

$$F(Q) = \frac{1}{N} \sum_{j=1}^N \langle \exp(-i\mathbf{Q} \cdot \mathbf{r}_j) \rangle, \quad (8)$$

where $\langle \dots \rangle$ denotes the average over multiple configurations of the particle. $F(Q)$ is referred to as the form factor amplitude for the collection of N nuclei, which comprise the particle/molecule of interest. Physically, because of the “phase problem,” we cannot directly measure this quantity and instead measure the complex square $P(Q) = F(Q)F^*(Q)$, where $F^*(Q)$ is the complex conjugate of $F(Q)$. This leads to a definition of the form factor

$$P(Q) = \frac{1}{N^2} \sum_{j=1}^N \sum_{k=1}^N \langle \exp[-i\mathbf{Q} \cdot (\mathbf{r}_j - \mathbf{r}_k)] \rangle. \quad (9)$$

In the continuous limit, Eqs. (8) and (9) can be recast in terms of the spatial density distribution of scattering sites $n(\mathbf{r})$ as

$$F(Q) = \frac{1}{N} \int \langle n(\mathbf{r}) \rangle \exp(-i\mathbf{Q} \cdot \mathbf{r}) d\mathbf{r}, \quad (10)$$

$$P(Q) = \frac{1}{N^2} \iint \langle n(\mathbf{r})n(\mathbf{r}') \rangle \exp[-i\mathbf{Q} \cdot (\mathbf{r} - \mathbf{r}')] d\mathbf{r}d\mathbf{r}'. \quad (11)$$

02 March 2025 18:16:14

For a particle with a uniform density, such as a sphere or rod, $\langle n(\mathbf{r}) \rangle$ reduces to a constant value, and $\langle n(\mathbf{r})n(\mathbf{r}') \rangle = \langle n(\mathbf{r}) \rangle \langle n(\mathbf{r}') \rangle$. This means that for objects with a uniform density, $P(Q) = |F(Q)|^2$. An example of calculating $F(Q)$ and $P(Q)$ for a sphere is shown in Appendix A. However, because polymer chains exhibit multiple configurations in solution and because monomer positions are correlated with one another, these simplifications do not apply to polymers. The configurational averages must be explicitly accounted for using an appropriate probability distribution for the polymer, as shown in Appendix C. Nevertheless, these expressions demonstrate that $F(Q)$ and $P(Q)$ are simply Fourier Transforms of $n(\mathbf{r})$ for the particle/polymer.

III. STANDARD PLOTS

SANS data can be analyzed by using two main methods: linear plots and nonlinear fits to appropriate models, as described above.^{39–43} In many instances, the first resort in analyzing SANS measurements is to observe the behavior of the data on so-called “standard plots” that can provide estimates of the fractal dimension and radius of gyration (R_g) of the scattering objects. Such plots do not require knowledge of the form factors but can yield valuable information on appropriate choices of form factors and length scales in the sample.

A. The Guinier plot

For a collection of N particles that make up a larger object, Debye⁴⁵ found that the form factor that describes the angular

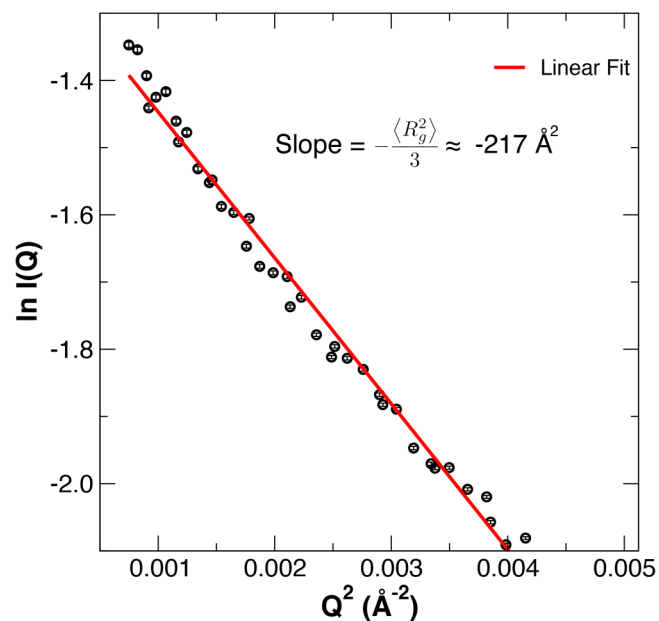


FIG. 4. Guinier plot of SANS data taken for $M_w = 11$ kg/mol polystyrene in cyclohexane at $T = 30$ °C. The slope of -217 \AA^2 implies an average radius of gyration of 2.5 nm.⁴⁴

dependence of the scattered neutron intensity can be expressed as a double sum,

$$P(Q) = \frac{1}{N^2} \sum_{i=1}^N \sum_{j=1}^N \frac{\sin(QR_{ij})}{QR_{ij}}. \quad (12)$$

If $QR_g < 1$, Eq. (12) can be expanded in a Taylor series to obtain the Guinier function,

$$\begin{aligned} P(Q) &= \frac{1}{N^2} \sum_{i=1}^N \sum_{j=1}^N \left[1 - \frac{(QR_{ij})^2}{3!} + \dots \right] \\ &= 1 - \frac{(QR_g)^2}{3} + \dots \approx \exp\left(-\frac{Q^2 \langle R_g^2 \rangle}{3}\right). \end{aligned} \quad (13)$$

The Guinier function is valid for dilute solutions at low- Q , independent of the shape of the particle, but does not explicitly account for polydispersity or interactions between particles in the sample.^{46,47} Under these conditions, the scattering intensity varies according to

$$I(Q) = I_0 P(Q) \approx I_0 \exp\left(-\frac{Q^2 \langle R_g^2 \rangle}{3}\right). \quad (14)$$

A plot of $\ln I(Q)$ as a function of Q^2 will yield the ensemble average $\langle R_g^2 \rangle/3$ as the slope, as shown in Fig. 4. If the shape of the particles in solution is known, e.g., spherical or cylindrical, then R_g^2 can be used to obtain the particle dimensions. For instance, if the particles are known to be rod-like on the basis of a Porod plot (discussed below), or complementary techniques, then $R_g^2 = R^2/2 + L^2/12$, where R and L are the average physical radius and length, respectively. Similarly, for spherical particles, the physical radius $R = \sqrt{5/3}R_g$. Other limiting cases, including thin rods ($R_g^2 = L^2/12$) and disks ($R_g^2 = R^2/12$), are straightforward to derive. A derivation of R_g for linear polymers in both the ideal and non-ideal limits is provided in Appendix B.

B. The Porod plot

The fractal dimension \mathcal{D} of a geometric shape characterizes the complexity of its structure. A straight line has fractal dimension $\mathcal{D} = 1$, while a 2D plane has $\mathcal{D} = 2$, and a uniform sphere has $\mathcal{D} = 3$. These values are only limiting cases, and the fractal dimension can assume non-integer values. For example, the coastlines of many nations have a fractal dimension between that of a straight line and a 2D surface due to roughness.⁴⁸ As $\mathcal{D} \rightarrow 1$, the coastline becomes increasingly smooth. Similarly, a rough surface will have a fractal dimension between that of a smooth plane ($\mathcal{D} = 2$) and a 3D object ($\mathcal{D} = 3$), and we refer to such surfaces as “surface fractals.” As $\mathcal{D} \rightarrow 2$, the surface becomes increasingly smooth. Finally, the mass contained within a particle may not be uniform, in which case the “mass fractal” can be characterized by a fractal dimension that describes how its mass scales with its size (i.e., the object’s dimensionality). In the case of polymer chains, it can be shown

that the fractal dimension $\mathcal{D} = 1/\nu$, where ν is the Flory exponent. For instance, a Gaussian polymer chain has $\mathcal{D} = 2$ since its size scales as $R \sim N^{1/2}$.

Scattering measurements at large values of Q provide information on a surface's fractal dimension. Porod⁴⁹ found that for large values of Q where length scales much smaller than the size of the particle are probed, the scattering intensity should decay as $I(Q) \sim Q^{-4}$ due to scattering from the sharp, smooth interface that separates the particle from its environment. Porod's approach can be generalized to rough or broad interfaces, in which case $I(Q) \sim Q^{-(6-\mathcal{D}_s)}$, where \mathcal{D}_s is the fractal dimension of the surface.²⁵ For a smooth surface or sharp interface, $\mathcal{D}_s = 2$, and Porod's original Q^{-4} scaling is recovered. For rough surfaces or broad interfaces, $2 < \mathcal{D}_s < 3$, and the scattering intensity will decay with an exponent between -3 and -4 in the surface fractal regime. Analysis of the surface fractal dimension is typically referred to as Porod analysis.

In an analogous way to Porod analysis, the mass fractal dimension can be observed by determining the exponent that describes the power law decay of the scattering intensity at values of Q that are larger than $1/R$ but sufficiently small that the particle surface is not being probed. From Eq. (11), the form factor is essentially the Fourier transform of $\langle n(\mathbf{r})n(\mathbf{r}') \rangle$. In other words, $I(Q) \propto \langle n(Q)n(-Q) \rangle$, where $n(Q)$ is the number of scattering sites within a region of size $Q = 1/r$. By definition, this quantity grows as $r^{\mathcal{D}}$, meaning that the intensity should decay as

$$I(Q) \propto \frac{C}{Q^{\mathcal{D}}}, \quad (15)$$

where C is a constant and \mathcal{D} is the fractal dimension of the mass fractal.³⁸ At low values of Q that correspond to length scales larger than the particle, $I(Q) \sim Q^0$ since $n(Q)$ saturates to the number of scattering sites within the particle [i.e., $I(Q)$ is constant]. For

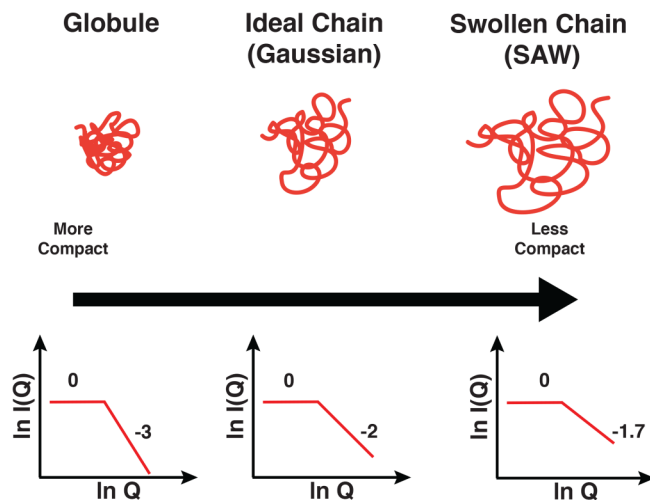


FIG. 5. Illustration of polymers with (left to right) globular, ideal, and swollen conformations. The corresponding Porod plots and slopes are shown below each.

polymer coils, whose size R scales with the molar mass as $R \sim M^\nu$, the intensity will decay as $Q^{-\mathcal{D}} = Q^{-1/\nu}$. As illustrated in Fig. 5, the value of the Porod exponent will depend on whether the coil is collapsed ($\nu < 1/2$), ideal ($\nu = 1/2$), or swollen ($\nu > 1/2$). Note that for particles with multiple length scales of interest, such as rods, the scattering data will exhibit two power law decays corresponding to the length of the rod [$I(Q) \sim Q^{-1}$] and the surface of the rod [$I(Q) \sim Q^{-4}$].^{29,50} A subtle, but important, point regarding values of the Porod exponent is that although, for example, the presence of an ideal coil implies that $I(Q) \sim Q^{-2}$, the reverse is not true. In other words, a Q^{-2} power law can originate from scattering of any object for which $\mathcal{D} = 2$, such as a flat sheet.

C. The Kratky plot

A Kratky plot, commonly implemented as a plot of $Q^2 I(Q)$ vs Q , emphasizes deviations from the high- Q behavior of the scattering intensity $I(Q)$. For polymer chains, the Kratky plot emphasizes the Gaussian chain nature or departure from it. Because $I(Q) \sim Q^{-2}$ for a Gaussian chain, a plateau is observed for large values of Q on the plot as shown in Fig. 6. Any positive deviation suggests that the chains are more swollen than in the Gaussian case, while a negative deviation suggests more collapsed structures. Based on this alone, it may seem that a Kratky plot does not yield additional information than the Porod plot does. However, for compact structures are present, the Kratky plot will show a peak. For example, star polymers with Gaussian arms will show a plateau at large values of Q , but a peak will appear at intermediate values of Q as the number of arms f increases due to the concentration of mass near the core of the molecule.⁵¹

IV. EMPIRICAL MODELS

By recognizing that Guinier's law provides R_g for an object, irrespective of its shape, and Porod's law provides the fractal

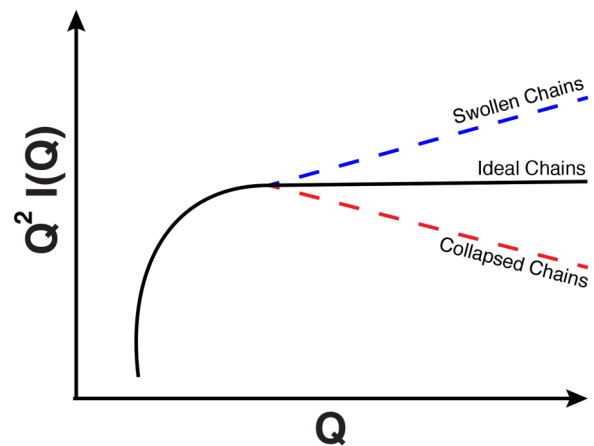


FIG. 6. Illustration of a Kratky plot for polymer chains in solution. Because $I(Q) \sim Q^{-2}$ for an ideal chain, the plot plateaus for large values of Q . For non-ideal chains, the plot deviates from this behavior—indicating that the chain is more swollen (top curve) or more collapsed (bottom curve) than an ideal chain.

02 March 2025 18:16:14

dimension of the object, it is possible to combine these descriptions into a single expression to model the decay of $I(Q)$ with Q . Two common approaches to this have been the unified scattering model from Beaucage⁵² and the Guinier–Porod model from Hammouda.⁵⁰ Although the two models are similar to one another, they differ primarily in how they connect the Guinier region to the Porod region.

A. Unified scattering model

Beaucage in 1995 derived a general approach that captures structural information at multiple length scales by combining the Guinier law with the generalized Porod law in Eq. (15).⁵² For a system that contains m length scales, the scattered intensity is modeled as

$$I(Q) = \sum_{i=1}^m \left[G_i \exp\left(-\frac{Q^2 R_{g,i}^2}{3}\right) + D_i \exp\left(-\frac{Q^2 R_{g,(i+1)}^2}{3}\right) \left(\frac{1}{Q_i}\right)^{D_i} \right] + B, \tag{16}$$

where increasing values of i correspond to larger length scales in the system and B is the incoherent background. From Eq. (16), it is clear that each structural level i contains four independent parameters: G_i , D_i , $R_{g,i}$, and D_i . The value Q_i^* is defined as

$$Q_i^* = Q \times \operatorname{erf} \left[\frac{kQR_{g,i}}{\sqrt{6}} \right]^{-3}, \tag{17}$$

where $k \approx 1$ is a constant that depends on the value of D_i . Least-squares fitting to the unified scattering model will produce a radius of gyration at each length scale as well as the Porod exponent. To illustrate the output of this model, the best fit to a 29 kg/mol polymer is shown in Fig. 7(a) as a red line, representing a globular object ($D = 2.55$) with $R_g \approx 3.5$ nm and a single characteristic length scale ($m = 1$). More complex objects, with hierarchical length scales, can be fit by including additional terms ($m > 1$) and by including terms describing correlations.^{52,55} Hammouda⁵⁶ analyzed the unified scattering model and noted that it works exceptionally well for describing the scattering from mass fractals and is particularly efficient in instances where averages over random orientations must be considered. However, he notes that to avoid artifacts introduced by letting both G_i and B_i vary independently, it may be best to relate the two values through an exact calculation of the form factor (see Table 2 in Ref. 56).

B. Guinier–Porod model

The Guinier–Porod model⁵⁰ is similar to the unified scattering model in that it links the Guinier and Porod regions of the scattering plot and can be extended to describe multiple length scales as well as more complicated systems such as polymer-grafted nanoparticles.⁵⁷ For the simplest case of a single length scale (i.e., $m = 1$ in the unified scattering model), the Guinier–Porod model is defined as

$$I(Q) = \begin{cases} \frac{G}{Q^s} \exp\left(\frac{-Q^2 R_g^2}{3-s}\right) + B, & Q \leq Q^* \\ \frac{D}{Q^D} + B, & Q > Q^* \end{cases} \tag{18}$$

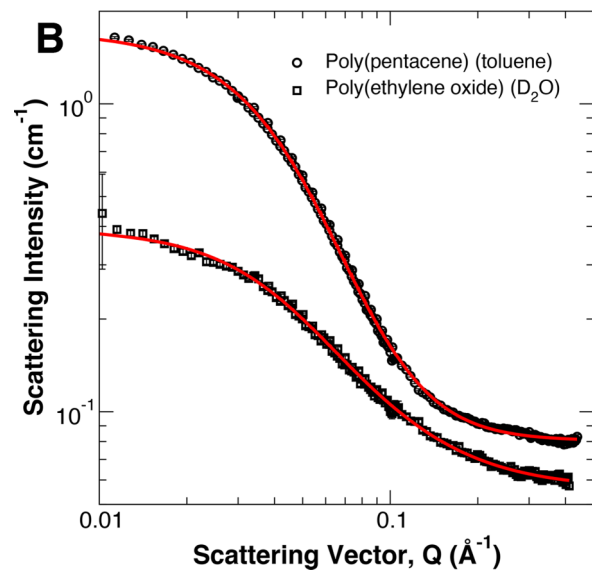
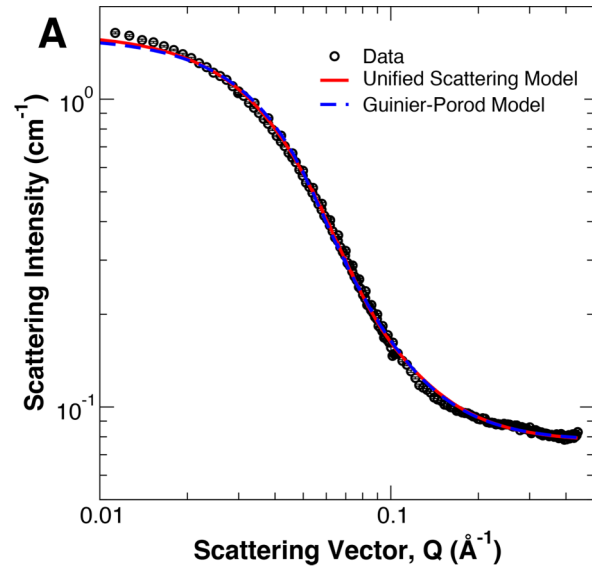


FIG. 7. (a) SANS measurements of a polymer with pendant pentacene groups⁵³ [poly(pentacene)] dissolved in d_8 -toluene, with fits using the unified scattering model [Eq. (16), red line] and the Guinier–Porod model [Eq. (18), blue dashes]. (b) Comparison of the scattering between poly(pentacene) and poly(ethylene oxide) (PEO) dissolved in D_2O .⁵⁴ The fits are to the form factor of a polymer with excluded volume, Eq. (26). Both polymers have $R_g \approx 3.5$ nm. For PEO, $\nu = 0.53$ ($D = 1.88$), while for poly(pentacene), $\nu = 0.39$ ($D = 2.55$).

where G and D are scaling factors, B is the incoherent background, and s is a dimensionless parameter that quantifies the shape of the objects. Specifically, $s = 0$ for spherical objects, $s = 1$ for rod-like objects, and $s = 2$ for planar or platelet-like objects, although

02 March 2025 18:16:14

non-integer values are possible. The Guinier and Porod regions are linked by requiring that the curves and their derivatives in those regions be equal and continuous at $Q = Q^*$, leading to

$$Q^* = \frac{1}{R_g} \sqrt{(D-s)(3-s)} \tag{19}$$

and

$$D = G \exp \left[-\frac{(D-s)}{2} \right] Q^{*(D-s)}. \tag{20}$$

By linking D and G in this manner, the number of free variables in the Guinier–Porod model is reduced. As a comparison to the unified scattering model, the best fit to a 29 kg/mol polymer is shown in Fig. 7(a) as a dashed blue line representing a globular polymer with $R_g = 3.5$ nm. The Guinier–Porod model and the unified scattering model are virtually identical. Hammouda⁵⁰ also demonstrated that the Guinier–Porod model can be extended to capture multiple length scales similar to the unified scattering model.

C. Correlation length models

Scattering measurements are very commonly performed to extract the size of density correlations, such as the average mesh size of a polymer network or the interfacial width of a two-phase system. In such situations, it can be useful to assume a functional form of the quantity of interest in real space and perform a Fourier transform to obtain a suitable scattering function, following Eq. (11). For example, in a two-phase system with a large domain size, if the density distribution function is assumed to decay exponentially at the interface with a decay length ξ , then the Fourier transform will result in

$$I(Q) = \frac{C}{(1 + Q^2\xi^2)^2} + B, \tag{21}$$

where B is the incoherent background and C is a scaling constant. This model is referred to as the Debye–Bueche or Debye–Anderson–Brumberger (DAB) model^{58,59} and provides the interfacial width ξ for systems such as phase separated polymer blends or porous materials. Notably, it also produces the Q^{-4} decay of the scattering intensity found by Porod for smooth interfaces.

If the correlations are assumed to decay as $n(r) \sim (1/r) \exp(-r/\xi)$ (i.e., an Ornstein–Zernike form⁶⁰), then the Fourier transform produces a Lorentzian in Q -space,

$$I(Q) = \frac{C}{1 + (Q\xi)^2} + B, \tag{22}$$

which is commonly used for measuring the mesh size of polymer networks.²⁵ However, the exponent in the denominator implies that the mass fractal dimension at intermediate values of Q is 2, which may not accurately reflect the structure being studied. To remedy this, the functional form of the Lorentzian can be generalized to describe a wider range of mass fractals, characterized by a fractal dimension D . Additionally, SANS measurements of polymer

networks may show a tail in the intensity at low- Q , which can be accounted for by introducing a power law term. In this case, the “correlation length model” is typically represented as⁶¹

$$I(Q) = \frac{A}{Q^n} + \frac{C}{1 + (Q\xi)^D} + B, \tag{23}$$

where A is a scaling constant. The first term of this equation describes scattering from a mass fractal at low values of Q (i.e., length scales much larger than the correlation length of interest), while the Lorentzian-like term represents density correlations with a size in real space of approximately ξ . The origin of the power law term may be large clusters/aggregates or the fractal structure of a polymer network over large length scales.

V. SCATTERING FROM LINEAR POLYMERS

In instances where the chemical composition and shape of the scattering object are known, more information can be garnered from scattering measurements by fitting the data using an appropriate scattering model rather than depending on empirical models or standard plots. Scattering from isolated polymer chains can be described using a combination of scattering factors, shown schematically in Fig. 8. The exact combination of these factors, which are derived in Appendix C, requires knowledge of the chemical composition of the polymer, architecture, and so on. For an isolated polymer chain, the angular dependence of the scattered neutrons depends on the form factor $P(Q)$. The form factor amplitude $F(Q)$ and correlations between chain ends, $E(Q)$, are necessary to describe block copolymers, grafted nanoparticles, and non-linear architectures. For solid objects, the form factor and form factor

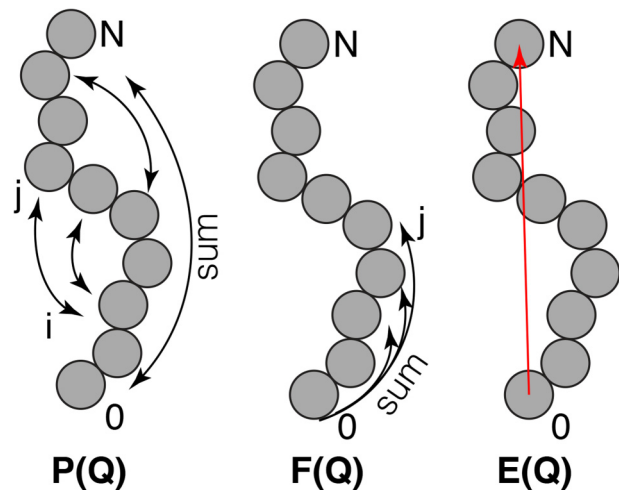


FIG. 8. Graphical representation of the three scattering factors for a polymer chain: (left) the form factor $P(Q)$ calculated from separations of all monomer pairs i, j , (center) the form factor amplitude $F(Q)$ calculated from the separations between all monomers j and the beginning of the chain, and (right) the chain end correlations $E(Q)$ calculated from only the positions of the first and last monomers of the chain.

02 March 2025 18:16:14

amplitudes are related as $P(Q) = |F(Q)|^2$. However, this relation does not apply to fractal chains, as shown in Appendix C. Nevertheless, knowing these three factors, it is possible to construct complex expressions for the scattering intensity of a given molecular species without the necessity of complicated calculations, as will be highlighted in Secs. V A and V B.

If interactions between a single polymer species and its environment are neglected, such is the case at the θ -temperature or in a melt of identical chains, the scattering intensity can be expressed as

$$I(Q) = A \times P(Q) + B, \quad (24)$$

where A is a scaling factor and B is the incoherent background. For an isotopically labeled polymer in a melt of identical chains, $A = \phi_p(1 - \phi_p)(\Delta\rho)^2 v_p$, where the contrast factor $\Delta\rho$ is the difference between the SLDs of the deuterated and hydrogenated chains and ϕ_p is the volume fraction of the labeled chains. For a polymer in a dilute solution, the equation is the previous one except $(1 - \phi_p) \approx 1$ due to the low concentration of polymers. In practice, it is common to simply let the prefactor A vary during the fitting process. In the presence of weak interactions, it may be possible to interpret the scattering measurement using Eq. (24), but it should be noted that values obtained for R_g , etc., will only be approximate. In principle, $I(Q=0)$ should be due only to scattering from the polymer and not vary significantly with temperature. However, as T increases, composition fluctuations increase in amplitude and must be accounted for using the random phase approximation (Sec. VIII). When composition fluctuations are non-negligible, the forward scattering intensity $I(Q=0)$ will increase as temperature increases for polymers showing lower critical solution temperature (LCST) behavior and decrease for those with upper critical solution temperature (UCST) behavior. If non-negligible composition fluctuations are not accounted for explicitly, one might arrive at incorrect conclusions for the scaling of the chain size with respect to temperature by using Eq. (24) alone. Regardless of whether or not one accounts for composition fluctuations, the largest obstacle in interpreting the scattering measurement is selection of a suitable function for $P(Q)$.

A. Homopolymers

The original Debye scattering function was derived in 1915 by Peter Debye, and for the interested reader, a derivation is provided in Appendix C of this Tutorial.⁶² Debye's work shows that scattering of radiation by molecules does not require that they form crystalline structures, as are commonly used for diffraction experiments. For polymer systems, the scattering from an isolated polymer chain with Gaussian statistics follows the Debye scattering function,

$$P(Q) = \frac{2}{(Q^2 R_g^2)^2} \left[\exp(-Q^2 R_g^2) + (Q^2 R_g^2) - 1 \right]. \quad (25)$$

However, in using this equation to interpret scattering measurements, it is important to note that, strictly speaking, it is only correct for the case that $\nu = 1/2$ and if the chain can be described by Gaussian statistics. This can be observed by considering the limit of Eq. (25) for $QR_g \gg 1$, where $P(Q) \sim 2/(R_g Q)^2$.⁴⁵ In this limit, the

Q^{-2} scaling is consistent with the previous discussion of Porod's law and shows that if the Flory parameter $\nu \neq 1/2$, that the high- Q scaling of the Debye function is not expected to correctly describe scattering from swollen or collapsed chains.

The Debye function correctly describes scattering from ideal chains—those chains that do not have excluded volume. The presence of favorable or unfavorable interactions between polymer and solvent will lead to positive or negative values for the excluded volumes of the monomers in the chain, respectively.⁶³ The main consequence of this is a Flory exponent $\nu > 1/2$ (favorable interactions) or $\nu < 1/2$ (unfavorable interactions), which in turn will affect the Porod exponent observed in scattering measurements. As shown in Appendix C, under the assumption that the chain is almost Gaussian, the form factor for a non-ideal chain can be expressed analytically in terms of the lower incomplete gamma function, $\gamma(d, x)$, as

$$P(Q) = \frac{1}{\nu U^{1/2\nu}} \gamma\left(\frac{1}{2\nu}, U\right) - \frac{1}{\nu U^{1/\nu}} \gamma\left(\frac{1}{\nu}, U\right) \quad (26)$$

to obtain the form factor for a polymer with excluded volume. This function applies for values of ν that are not too far from $1/2$ and has been used by the authors on the interval $\nu \in (0.3, 0.8)$ to achieve reasonable results. Notably, this form factor does not apply in the limit of $\nu = 1$, and in such a case, the form factor for a thin rod is more appropriate. Fits to SANS measurements of two polymers—a 29 kg/mol poly(pentacene) and an 11 kg/mol poly(ethylene oxide)—using the form factor in Eq. (26) are shown in Fig. 7(b).

B. Linear multi-block copolymers

Using the scattering terms shown in Fig. 8, it is possible to construct form factors for more complex polymer architectures without the need for lengthy derivations.⁶⁴ As an illustration of this process, the form factors for a diblock and triblock copolymer are derived in this section. This method can be extended to other related architectures. If the form factor is thought of as a coherent sum of the form factor amplitudes of each component, each weighted by the degree of polymerization of the respective block, the form factor $P_{AB}(Q)$ of an A-B diblock copolymer can be expressed as

$$P_{AB}(Q) = |N_A F_A(Q) + N_B F_B(Q)|^2 \quad (27)$$

$$= N_A^2 |F_A(Q)|^2 + N_B^2 |F_B(Q)|^2 + 2N_A N_B F_A(Q) F_B(Q), \quad (28)$$

where N_A and N_B are the degree of polymerization of blocks A and B, respectively. Equation 28 is almost the final expression, but the substitution $|F_i(Q)|^2 \rightarrow P_i(Q)$ must be made for the square of each form factor amplitude, following the discussion in Appendix C. In addition, each form factor amplitude should be weighted by the contrast $\Delta\rho$ and each form factor by $\Delta\rho^2$. $P_i(Q)$ can be obtained from Eqs. (25) or (26), and the form factor of the diblock (neglecting the contrast terms) becomes

$$P_{AB}(Q) = N_A^2 P_A(Q) + 2N_A N_B F_A(Q) F_B(Q) + N_B^2 P_B(Q). \quad (29)$$

Equation (29) can be thought of as arising from the combination of an A homopolymer with a correlation term $F_A(Q)F_B(Q)$, as well as a B homopolymer with a similar correlation term (hence, the factor of 2). A graphical representation of the construction of $P_{AB}(Q)$ is shown in Fig. 9.

The construction of the form factor for an ABC triblock copolymer follows a similar process. However, because the A and C blocks are not directly connected to one another, a propagation factor $E(Q) = \exp(-Q^2 R_{g,B}^2)$ is needed, which represents correlations between the ends of the A and C blocks, separated approximately by the radius of gyration of the B block, $R_{g,B}$. If N_i is the degree of polymerization of block i , then the triblock form factor $P_{ABC}(Q)$ is constructed as

$$\begin{aligned}
 P_{ABC}(Q) &= |N_A F_A(Q) + N_B F_B(Q) + N_C F_C(Q)|^2 \quad (30) \\
 &= |N_A F_A(Q)|^2 + |N_B F_B(Q)|^2 + |N_C F_C(Q)|^2 \\
 &\quad + 2N_A N_B F_A(Q) F_B(Q) + 2N_A N_C F_A(Q) E(Q) F_C(Q) \\
 &\quad + 2N_B N_C F_B(Q) F_C(Q), \quad (31)
 \end{aligned}$$

where the substitution $F_A(Q)F_C(Q) \rightarrow F_A(Q)E(Q)F_C(Q)$ was made to account for the fact that the A and C blocks are not connected to one another. The contrast factors $\Delta\rho$ have been omitted for clarity but should be included in the same manner as described for the diblock case. After substituting $P_i(Q)$ [cf. Eq. (25) or (26)] for the squares of the form factor amplitudes of each block, the resulting form factor is

$$\begin{aligned}
 P_{ABC}(Q) &= N_A^2 P_A(Q) + N_B^2 P_B(Q) + N_C^2 P_C(Q) \\
 &\quad + 2N_A N_B F_A(Q) F_B(Q) + 2N_A N_C F_A(Q) E(Q) F_C(Q) \\
 &\quad + 2N_B N_C F_B(Q) F_C(Q) \quad (32)
 \end{aligned}$$

An illustration of the terms of $P_{ABC}(Q)$ is shown in Fig. 10. Construction of form factors for linear block polymers with a larger number of blocks follows a similar process and will involve a larger number of propagating terms, $E(Q)$.

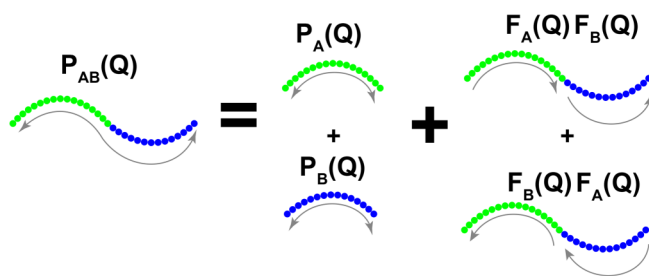


FIG. 9. Decomposition of the form factor of an AB diblock copolymer. Taking the amplitude of the coherent sum of the form factor amplitudes of each block $P_{AB}(Q) = |F_A(Q) + F_B(Q)|^2$ results in four terms with the substitution $|F_i(Q)|^2 = P_i(Q)$.

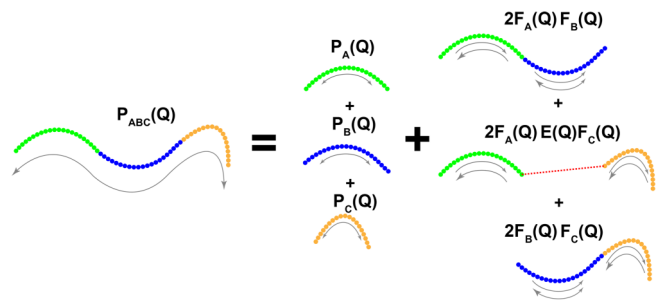


FIG. 10. Decomposition of the form factor of an ABC triblock copolymer. Taking the amplitude of the coherent sum of the form factor amplitudes of each block $P_{ABC}(Q) = |F_A(Q) + F_B(Q) + F_C(Q)|^2$ results in six terms with the substitution $|F_i(Q)|^2 = P_i(Q)$ and $F_i(Q)F_j(Q) = F_i(Q)E(Q)F_j(Q)$ for blocks that are not adjacent, where $E(Q)$ is the correlation between the chain ends of blocks i and j .

VI. COMPLEX POLYMER ARCHITECTURES

A. Star polymers

A natural extension to the consideration of multiblock polymers is to consider the case of polymers where all blocks are connected to a central junction. These “star polymers” consist of f arms connected to a central core. The arms may be chemically identical or block copolymers.⁶⁵ In the case of miktoarm (“mixed arm”) polymers, the arms may have different chemical compositions from one another. Interpreting SANS measurements from such polymers is possible, and the approach to constructing expressions for $P(Q)$ is somewhat similar to the case of homopolymers and block copolymers.

The classical form factor for the star polymer form factor is due to Benoit.⁶⁶ Early investigations by Willner *et al.* applied the Benoit star form factor to investigate the conformation of star polymers with functionalities ranging from $f = 8$ to 128 arms in a good solvent.¹³ The authors found that the star form factor described the data well for small values of f ; however, as $f \rightarrow 128$, the data were more similar to the form factor of a sphere. Thus, one should take into consideration the number of arms of the star polymer when deciding on the appropriate model to use, and standard plots can assist in making a suitable selection.

As in the case of linear polymers, the classical form factor is only true in the case of $\nu = 1/2$, where the arms are described by Gaussian statistics. Lang *et al.* extended the form factor to account for a general value of ν using the form factor for a polymer chain with excluded volume. In their work, they investigated the conformation of PNIPAM star polymers with $f = 3-6$ in water with different functional end groups.⁶⁷ The construction of the form factor for a star polymer follows a similar approach regardless of whether the polymers are assumed to be ideal or have excluded volume contributions.

The form factor for one arm of the star polymer is assumed to be described by either Eqs. (25) or (26). In this case, the form factor for a star polymer with f arms having a degree of polymerization N is

02 March 2025 18:16:14

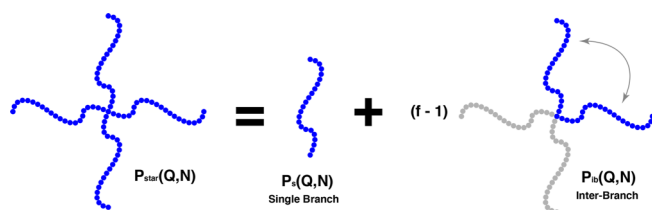


FIG. 11. Decomposition of the form factor of a star polymer with $f = 4$ arms/branches. The scattering is described by that from each arm, as well as $(f - 1)$ inter-branch correlation terms.

$$P_{star}(Q, N) = \frac{1}{f} \left| \sum_{i=1}^f F_i(Q) \right|^2 = \frac{1}{f} [P_s(Q, N) + (f - 1)P_{ib}(Q, N)], \quad (33)$$

where $P_{ib}(Q, N) = F_i(Q, N)F_j(Q, N)$ is the correlation between arms $i \neq j$, of which there are $(f - 1)$ factors. If the arms are chemically distinct from one another, the form factor amplitudes should again be weighted by their associated contrast factor. The terms of Eq. (34) are illustrated in Fig. 11. Hammouda^{51,67} noted that rather than multiply the form factor amplitudes of arms i and j , it is possible to use an equivalent form where $P_{ib}(Q, N) = 2P_s(Q, 2N) - P_s(Q, N)$ by analogy to the binomial expansion [i.e., $2ab = (a + b)^2 - a^2 - b^2$]. An analysis of SANS measurements using this model fits the data well and produced values of R_g that were in good agreement with known values from linear polymers.⁶⁷

Although these form factors have been successful in modeling the scattering from star polymers, it is worth noting that other, more advanced approaches exist. In particular, Alessandrini and Carignano⁶⁸ used renormalization group techniques to obtain the scattering functions for a star polymer. While powerful, this approach is significantly more difficult to develop than the simple approach outlined here. However, it has advantages over the Benoit form factor in that it captures the effects of excluded volume without the approximations required in Appendix C. In this sense, the renormalization group approach may be a more accurate description of the scattering characteristics.

B. Cyclic/ring polymers

Recently, cyclic polymers have received increasing attention in the polymer community because of their biological relevance and interesting rheological properties.^{69,70} In addition, the recent report of the synthesis of linear poly[n]catenane molecules,⁷¹ which consist of a series of mechanically interlocked rings, has further motivated the investigation of rings and ring-like structures. Some of the most recent SANS results regarding the structure of cyclic polymers include the fact that the rings tend to be more swollen than their linear counterparts and can be swollen by linear chains.^{44,72,73}

Cyclic polymers can be studied with empirical models and standard plots. However, knowledge of the form factor can be used

to extract thermodynamic information and better understand the scaling of the chain with N . The form factor of a cyclic polymer is more complicated than that of linear or star polymers and can be calculated numerically from its definition,^{44,51}

$$P(Q) = 2 \int_0^1 ds (1 - s) \exp[-s^{2\nu}(1 - s^{2\nu})U], \quad (34)$$

where $U = QR_g/2$ and s represents the position along the contour of the ring. Currently, an analytical expression has not been found, although in the limiting case of $\nu = 1/2$, the form factor can be expressed in terms of Dawson's integral^{51,74} $D(QR_g/2)$ as

$$P_{ring}(Q) = 2 \frac{D(QR_g/2)}{QR_g}, \quad (35)$$

where Dawson's integral is defined as

$$D(x) = \exp(-x^2) \int_0^x \exp(t^2) dt. \quad (36)$$

C. Bottlebrush polymers

Bottlebrush polymers consist of a series of macromonomers (i.e., polymer chain building blocks), which are polymerized along a common backbone. The close proximity of the side chains on the backbone results in strong steric repulsion, which in turn results in a long, cylinder-like molecule with a diameter that is on the order of the length of the macromonomers. Interpretation of SANS measurements of bottlebrushes, so far, relied on two primary approaches: fits to the Guinier-Porod model and/or fits to a flexible cylinder model.^{75,76} Beers and co-workers found that SANS from bottlebrushes could be fit by a product of an infinitely thin cylinder, representing the backbone of the polymer, and a term describing scattering from the cross section of the bottlebrush.⁷⁷

VII. MICELLES AND POLYMER-GRAFTED NANOPARTICLES

There has been much focus in recent years on understanding the structure of polymers that are grafted to nanoparticle surfaces, and SANS has proven to be a useful method for making such measurements.²¹ In fact, this is maybe not so surprising given the large body of work in the literature that has used SANS to probe the structure of micelles. Polymer-grafted nanoparticles, micelles, and even star polymers share many common physical characteristics that aid in developing models of their scattering.

Pedersen originally developed a suite of scattering models to interpret scattering from block copolymer micelles⁷⁸ and similar structures.⁷⁹ A key assumption in using the Debye function in the original "core-chain" model is that for the polymers in the corona of the micelle, $\nu = 1/2$. Measurements of such systems benefit from moving to dilute solutions, in which case the interparticle structure factor, which describes the positions of the particles relative to one another, vanishes [i.e., $S_I(Q) \approx 1$]. In this limit, the

scattering from a solution of particles is written as

$$I(Q) = \phi_N V^2 \Delta\rho^2 P(Q) S_I(Q) \approx \phi_N V^2 \Delta\rho^2 P(Q), \quad (37)$$

where ϕ_N is the number density of particles in the solution, V is the total particle volume, and $\Delta\rho$ is the contrast factor defined earlier. In the event that $S_I(Q) \neq 1$, a suitable choice of the structure factor must be included, as was done in Ref. 83, for example. This leaves only the form factor to be determined in order to interpret a SANS measurement.

In Pedersen's approach, the form factor can be derived in a similar way as the form factor for a star polymer. This approach is advantageous in that it can be extended to several related systems. The starting point in developing core-chain models is to write the form factor in terms of the form factor amplitudes of each component, absorbing the volume and contrast terms from Eq. (37) into $P_{cc}(Q)$,

$$P_{cc}(Q) = \left| V_c \Delta\rho_{c,s} F_c(Q) + V_p \Delta\rho_{p,s} \sum_{i=1}^{N_g} F_p(Q) \right|^2, \quad (38)$$

where $F_c(Q)$ is the form factor amplitude of the core, $F_p(Q)$ is the form factor amplitude for a grafted chain, and N_g is the number of chains grafted to the nanoparticle. In addition, $\Delta\rho_{c,s}$ is the difference in SLDs between the core and solvent and $\Delta\rho_{p,s}$ is the difference in SLDs between the grafted chains and the solvent. Finally, the terms are weighted by their relative volumes V_c and V_p . For the core-chain model, $F_c(Q) = 3j_1(QR_c)/QR_c$, where $j_1(x)$ is a spherical Bessel function. The origin of this term is described in detail in Appendix A. Note that the core-shell-chain model⁸⁰ can be obtained by substituting the form factor amplitude for a core-shell sphere into Eq. (38).

When Eq. (39) is expanded, four terms appear due to the fact that all of the polymer chains are assumed to be identical. The four terms are shown schematically in Fig. 12 and read

$$P_{cc}(Q) = \left[V_c^2 \Delta\rho_{c,s}^2 P_c(Q) + N_g V_p^2 \Delta\rho_{p,s}^2 P_p(Q) + 2N_g V_c V_p \Delta\rho_{c,s} \Delta\rho_{p,s} F_c(Q) E(Q) F_p(Q) + N_g(N_g - 1) \Delta\rho_{p,s}^2 V_p^2 F_p(Q) E^2(Q) F_p(Q) \right], \quad (39)$$

where $E(Q) = j_0(QR_c) = \sin(QR_c)/QR_c$ is a propagating factor, obtained in an analogous way to that shown in Appendix C, R_c is the radius of the core, and the substitution $|F_i(Q)|^2 \rightarrow P_i(Q)$ has been made. Although Eq. (40) appears to depend on a large number of terms, if the size of the core, polymer grafting density, and polymer molecular weight are known, the form factor depends primarily on the radius of gyration of the grafted chains and v . More advanced functions can be derived, such as those for elliptical or cylindrical cores,⁷⁹ grafted block copolymers (the "core-chain-chain" model),^{22,35} or particles with loopy coronas.⁸¹ These models may connect naturally to thermodynamic quantities such as the Flory-Huggins parameter χ or the second virial coefficient A_2 . In fact, Wei *et al.* demonstrated that the core-chain-chain model can be connected to thermodynamic

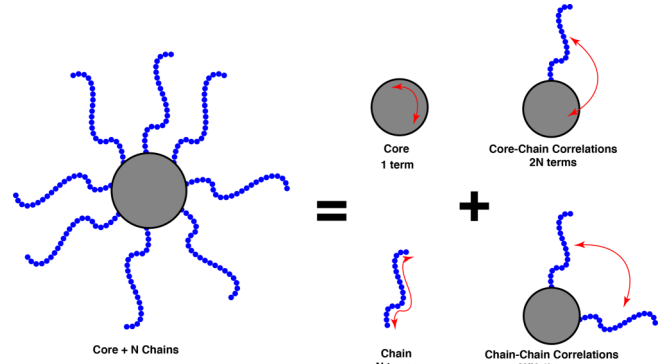


FIG. 12. Decomposition of the core-chain form factor into four primary terms, corresponding to scattering from the core and grafted polymers, and two correlation cross-terms.

quantities of the system through the Flory-Rehner equation.²² Recently, Hammouda and Kim derived an empirical core-chain model that combines many features of the Guinier-Porod model with the core-chain approach, resulting in a simpler model that describes spherical, polymer-grafted particles with good accuracy.⁵⁷ By replacing the form factor and form factor amplitudes of the polymer chains by those for small spheres, Pozzo and co-workers were able to derive a "raspberry" model to describe Pickering emulsions.⁸² This model was also useful for interpreting SANS from polymer-grafted virus-like particles.⁵⁴

A comparison between SANS from isolated poly(*N*-cyclopropylacrylamide) (PNCAPAM, $M_n = 21$ kg/mol) chains in solution and self-assembled PNCAPAM micelles is shown in Fig. 13(a), along with fits to the appropriate form factors.⁸³ The scattering intensity from the micelles is much larger in intensity than for the free chains and exhibits a steeper slope at intermediate values of Q , which implies the presence of more compact objects. The small peak in the scattering intensity of the micellar system is due to the presence of a non-negligible structure factor term. Nevertheless, the core-chain model fits the SANS measurements well.

VIII. ADVANCED MEASUREMENT TECHNIQUES

Much of the discussion in this Tutorial has so far focused on the angular dependence of the scattered neutron intensities, which are captured by the form factor. Although this represents the bulk of interpreting many conventional SANS measurements, and under certain conditions, it is necessary to consider the influence of interactions between the polymer and solvent (random phase approximation) or to take advantage of more intricate deuteration conditions (zero average contrast) to highlight scattering from the polymers of interest.

A. The random phase approximation (RPA)

At low temperatures, composition fluctuations due to thermal energy in the system are small. If these fluctuations are sufficiently

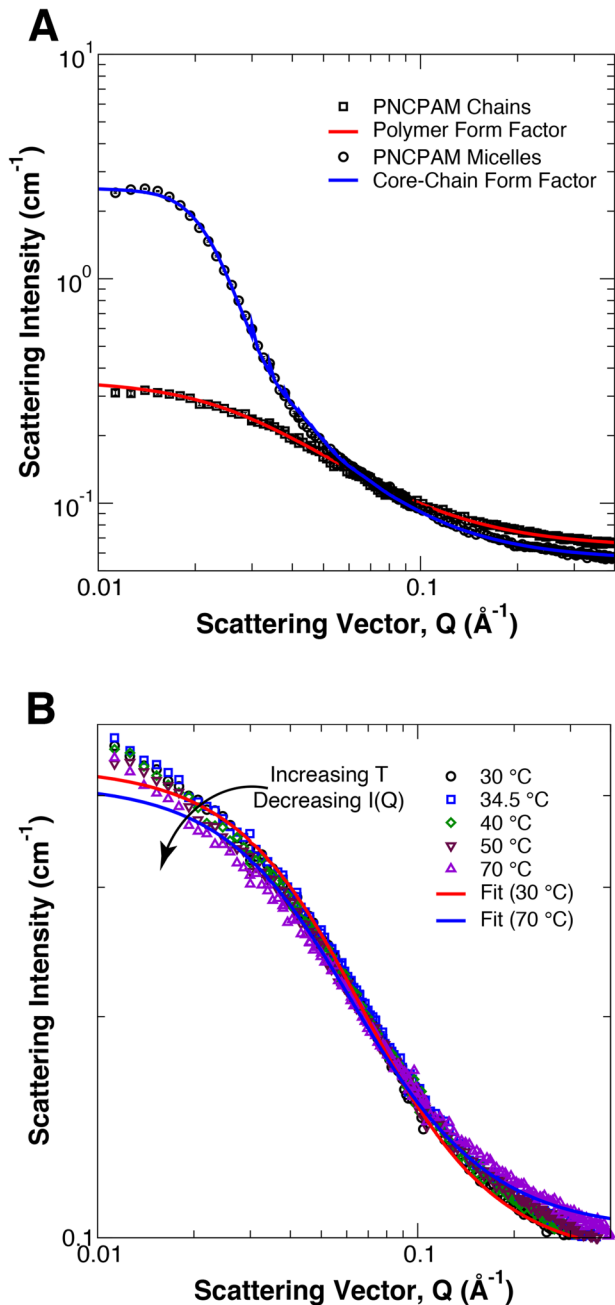


FIG. 13. (a) Comparison between scattering from isolated poly (*N*-cyclopropylacrylamide) (PNCPAM) polymers in solution ($M_n = 21$ kg/mol) and micelles composed of self-assembled PNCPAM chains.⁸³ The polymers are fit to the form factor of a polymer with excluded volume [Eq. (26)], while the micelles are fit to the core-chain model [Eq. (40)]. (b) SANS measurements of 11 kg/mol linear polystyrene dissolved in d_{12} -cyclohexane as a function of temperature. The scattering intensity decreases as T increases due to more favorable interactions between the polymer and the solvent. The solid lines are fits to the data using the RPA at $T = 30$ °C (red) and $T = 70$ °C (blue).

small, then $I(Q)$ is due only to the structure of the polymer chain, $I(Q) \approx AP(Q)$, and the approaches discussed in Secs. III–VII of this Tutorial can be used to interpret SANS measurements. However, the sizes of these fluctuations increase with temperature and become an increasingly non-negligible contribution to $I(Q)$. As composition fluctuations grow in size, $I(Q)$ depends on both the structure of the polymer as well as composition fluctuations in the scattering volume. In the limit of weak fluctuations, $I(Q \rightarrow 0) \sim (T - T_c)^{-1}$, and the Random Phase Approximation (RPA) must be used to correctly account for such effects.^{10,60,84} Close to T_c , strong fluctuations lead to deviations from the mean-field (Flory–Huggins) description of the system, and the RPA no longer applies. Such a deviation would be apparent in a non-linear scaling of $I(0)$ with $1/T$. To evaluate whether the mean-field description is valid, one can use the Ginzburg criterion.^{38,84} Typically, for high molecular weight polymer blends, the mean-field description is valid over a wide temperature range since the size of the fluctuations $\langle(\delta\phi)^2\rangle \sim 1/N$.³⁸ In contrast, the mean-field region for polymer solutions is smaller, although its exact size depends on the molecular weight of the polymer and the proximity to the critical point.

Since the scattering intensity depends on the average number of monomers within the scattering volume, it is relatively straightforward to show that $I(Q \rightarrow 0) = k_B T (\partial \Delta F_{mix} / \partial \phi^2)^{-1}$, where ΔF_{mix} is given by the Flory–Huggins equation.³⁸ A full Q -dependent treatment of composition fluctuations is beyond the scope of this Tutorial but can be found elsewhere.^{60,84} The result of this treatment (the “Random Phase Approximation”) expresses the scattering intensity as

$$I(Q) = \left[\frac{1}{\phi V_A P_A(Q)} + \frac{1}{(1-\phi) V_B P_B(Q)} - \frac{2\chi}{v_0} \right]^{-1}, \quad (40)$$

where ϕ is the volume fraction of component A, V_A and V_B are the molecular volumes of the A and B components, χ is the Flory–Huggins interaction parameter, and v_0 is a reference volume. Note that if B is assumed to be a solvent, $P_B(Q) = 1$. Although the RPA was derived for polymers that exhibit Gaussian statistics (i.e., $\nu = 1/2$), reasonable results have been obtained when the form factor for a polymer with excluded volume [Eq. (26)],⁸⁵ a star polymer [Eq. (34)],⁶⁷ or a ring [Eq. (35)] is used.⁴⁴ However, it should be noted that the expression is only an approximation in these limits. Beyond binary mixtures, the RPA has been extended to describe ternary systems, such as in studies of PNIPAM con-solvency in mixed solvents⁸⁵ as well as block copolymer systems.⁸⁶

SANS measurements of linear polystyrene ($M_n = 11$ kg/mol) in deuterated cyclohexane are shown in Fig. 13 as a function of temperature. The scattering intensity at low- Q decreases as T increases because the interaction parameter χ decreases with T , characteristic of UCST behavior. Fits to the RPA using Eq. (41) with the form factor of a polymer with excluded volume [Eq. (26)] are shown as solid lines. The data at $T = 30$ °C are the same data used to construct the Guinier plot in Fig. 5.

B. Zero average contrast (ZAC) conditions

A final technique that has proved to be indispensable for studying polymer systems is the Zero Average Contrast (ZAC) method.³⁷ The ZAC approach involves combining a mixture of deuterated and hydrogenated polymers with a mixture of deuterated and hydrogenated solvents with the goal of isolating scattering from single chains only. The approach is particularly useful for high concentrations of polymers and for measuring polymers that may cluster/aggregate in solution, such as PNIPAM.⁸⁵ In the case of PNIPAM, which becomes increasingly aggregated as T increases, aggregation of chains leads to an apparent increase in the radius of gyration of the polymers (independent of the interaction considerations discussed above) despite the chains being known to collapse with increasing temperature.⁸⁸ Applying the ZAC condition essentially reduces the problem of interpreting scattering from a ternary system to a simpler, effective binary system.⁸⁷

In this case, the intensity $I(Q)$ contains a term proportional to the polymer's form factor, as well as a term containing interchain correlations,

$$I(Q) = AP_S(Q) + CP_T(Q) + B, \quad (41)$$

where $P_S(Q)$ is the single-chain form factor and $P_T(Q)$ contains contributions to the scattering beyond the scattering of the particle of interest. ZAC is used to attempt to eliminate their contributions to the measured scattering. If the SLDs of the deuterated polymer (ρ_{dP}), hydrogenated polymer (ρ_{hP}), and solvent mixture (ρ_S) are accounted for, the scattering intensity is^{87,88}

$$I(Q) = (\rho_{dP} - \rho_{hP})^2 \frac{\phi_{dP}\phi_{hP}}{\phi_P^2} n_P \phi_P v_P P_S(Q) + (\rho_P - \rho_S)^2 n_P \phi_P v_P P_T(Q) + B, \quad (42)$$

where B is the incoherent background. The SLD of the isotopic mixture of polymers is given by $\rho_P = [\rho_{dP}\phi_{dP}/\rho_P + \rho_{hP}(1 - \phi_{dP})/\phi_P]$, where ϕ_P is the volume fraction of the total polymer relative to the solvent and ϕ_{dP} is the volume fraction of deuterated polymer relative to the hydrogenated polymer. Similarly, the SLD of the isotopic solvent mixture can be calculated as $\rho_S = [\rho_{dS}\phi_{dS}/(1 - \phi_P) + \rho_{hS}(1 - \phi_{dS})/(1 - \phi_P)]$, where ϕ_{dS} is the volume fraction of the deuterated solvent relative to the hydrogenated solvent. Although these expressions are involved, the goal of a ZAC measurement is to choose $\rho_P = \rho_S$ such that the second term of Eq. (42) vanishes. Although this condition can be estimated by calculating the SLDs of all components, in practice, it is best to determine the ZAC condition through experimental measurements. A full discussion is beyond the scope of this Tutorial, but in-depth discussions and examples are available elsewhere.⁸⁷⁻⁹⁰

IX. CONSIDERATIONS FOR FITTING DATA

The majority of the models described above require fitting SANS data with a least-squares method in a suitable software package. In doing this, there are many factors that must be considered such as whether the model is an accurate description for the particles/molecules of interest, whether there are impurities or

aggregates that influence the shape of the scattering curve, whether the fitted parameters make physical sense, and whether the fitted model is a “good fit” to the data. Although a complete discussion of fitting data is beyond the scope of this Tutorial, there are a few metrics by which a user can evaluate their analysis of a measurement.

The first metric is the reduced “chi-squared,” χ_R^2 , where

$$\chi_R^2 = \frac{1}{(N_{pts} - N_{par})} \sum_{i=1}^{N_{pts}} \frac{(I_{i,exp} - I_{i,theo})^2}{w_i^2}. \quad (43)$$

In the above expression, I_{exp} is the set of experimentally measured points and I_{theo} is the calculated value from the chosen model. The weights w_i are the error in I_{exp} and can be provided with the experimental measurement (typical) or calculated from the square root of I_{exp} . N_{pts} is the number of experimental points and N_{par} is the number of free parameters. Ideally, $N_{pts} \gg N_{par}$. For a “good fit,” $\chi_R^2 \rightarrow 1$, although because of low- Q tails and other artifacts in the data, it may not be possible to achieve such a low value in practice. Similarly, if $\chi_R^2 < 1$, the data have been over-fit.⁹¹

Another metric that can be used to assess the quality of the fit is the residuals after fitting. This may be especially useful in evaluating the quality of a fit in a certain Q -range. The residual for each data point i is calculated as

$$R_i = \frac{I_{i,exp} - I_{i,theo}}{w_i}. \quad (44)$$

If 68% of the residuals fall within one standard deviation, then $R_i \in [-1, 1]$. Residuals that fall outside of $[-3, 3]$ are a sign that the model does not accurately describe the data, and the set of parameters and/or model should be reconsidered.

X. CONCLUSIONS AND FUTURE OUTLOOK

Small-angle scattering, and, in particular, small-angle neutron scattering, will continue to be a powerful technique for measuring the conformation, size, and thermodynamic properties of polymer systems. In this Tutorial, we have focused primarily on the minimum necessary concepts that will allow new users of the technique to prepare appropriate samples for SANS measurements and interpret the results of their measurements. SANS, in general, is broadly applicable to polymer solutions, melts, and gels, as well as particulate systems including polymer-grafted nanoparticles and micelles. It should also be noted that much of the discussion in this Tutorial is also applicable to small-angle x-ray scattering (SAXS) measurements.

Looking to the future, there are numerous opportunities for extending the available models and current approaches to analyzing SANS measurements. For example, more refined, analytical form factors for bottlebrushes and polymer-grafted nanorods would be a significant advance in our ability to understand the behavior of those systems—including the structure and dynamics of the side chains or grafted polymers. In addition, we have noted throughout this Tutorial situations where analytical expressions are, to the best of our knowledge, not available. For this reason, numerical models, machine learning, and artificial intelligence may be alternate

approaches to interpreting SANS measurements.⁹² One such technique, Computational Reverse-Engineering Analysis for Scattering Experiments (CREASE), is a relatively new approach that can reconstruct a molecular picture of micellar structures *in silico* from experimental SANS data.⁹³ However, for those situations in which a suitable form factor is not available, the shape-independent functions (e.g., Unified Scattering Model) and standard plots that we have highlighted in this Tutorial can yield valuable information on samples of interest.

Finally, although we have attempted to make this Tutorial relatively self-contained for the new user, the topics that we have covered here are only a subset of a very rich field. Other resources, such as *The SANS Toolbox*,²⁵ the monograph by Higgins and Benoit,²⁴ and many reviews and perspectives in the literature can provide additional insights into more advanced topics.

ACKNOWLEDGMENTS

The authors thank Dr. Boualem Hammouda (NIST Center for Neutron Research, NCNR) for years of helpful discussions in developing new scattering models and for authoring *The SANS Toolbox*, which inspired several sections of this Tutorial. The authors also thank the National Science Foundation (NSF, No. DMR-2010792) for its support of the Center for High Resolution Neutron Scattering (CHRNS) at the NCNR, as well as for supporting the CHRNS Summer School on Neutron Scattering that the authors both attended.

APPENDIX A: THE FORM FACTOR OF A SPHERE

As an example of the application of Eq. (10) for calculating the form factor amplitude/form factor of an object with uniform volume, consider the case of a sphere with radius R_s . Since the density is constant throughout the particle, $\langle n(\mathbf{r}) \rangle = n/V_s$ for $r < R_s$ and $n(\mathbf{r}) = 0$ for $r > R_s$. With this, the form factor amplitude in spherical coordinates can be written as

$$F(Q) = \frac{3}{4\pi R_s^3} \int_0^{2\pi} d\phi \int_0^{R_s} r^2 dr \int_0^\pi \exp(-i\mathbf{Q} \cdot \mathbf{r}) \sin \theta d\theta. \quad (A1)$$

Replacing the dot product by $\mathbf{Q} \cdot \mathbf{r} = Qr \cos \theta$, evaluating the integral over ϕ , and letting $\mu = \cos \theta$, this expression simplifies to

$$F(Q) = \frac{3}{2R_s^3} \int_0^{R_s} r^2 dr \int_1^{-1} \exp(-iQr\mu) d\mu \quad (A2)$$

$$= \frac{3}{2R_s^3} \int_0^{R_s} r^2 \left[\frac{\cos(Qr\mu)}{-iQr} - \frac{\sin(Qr\mu)}{Qr} \right]_{\mu=1}^{\mu=-1} dr \quad (A3)$$

$$= \frac{3}{R_s^3} \int_0^{R_s} r^2 \frac{\sin(Qr)}{Qr} dr = \frac{3j_1(QR_s)}{QR_s}, \quad (A4)$$

where $j_1(x)$ is a spherical Bessel function. The form factor $P(Q) = |F(Q)|^2$.

APPENDIX B: $\langle R_g^2 \rangle$ FOR POLYMER CHAIN WITH EXCLUDED VOLUME

Here, we derive the expression for the mean-squared radius of gyration of a polymer chain for any value of the Flory exponent ν . For a polymer with excluded volume, the mean-squared distance between two monomers i and j is assumed to take the form

$$\langle r_{ij}^2 \rangle = b^2 |i - j|^{2\nu}, \quad (B1)$$

where b is the Kuhn length and the Flory exponent takes on limiting values of $\nu = 1/3$ for a globular structure, $\nu = 1/2$ for a Gaussian chain, and $\nu \approx 3/5$ for a swollen chain. Then, by definition, the mean-squared radius of gyration can be computed³⁸ according to

$$\langle R_g^2 \rangle = \frac{1}{N^2} \sum_{i=1}^N \sum_{j=i}^N b^2 (j - i)^{2\nu}, \quad (B2)$$

which eliminates the use of the absolute value function. In the continuous limit, Eq. (B2) can be cast into an equivalent form

$$\langle R_g^2 \rangle = \frac{b^2}{N^2} \int_0^N du \int_u^N (w - u)^{2\nu} dw. \quad (B3)$$

Evaluating this integral yields

$$\langle R_g^2 \rangle = \frac{b^2}{N^2} \int_0^N \frac{(N - u)^{2\nu+1}}{(2\nu + 1)} du = \frac{b^2 N^{2\nu}}{(2\nu + 1)(2\nu + 2)}. \quad (B4)$$

Note that for $\nu = 1/2$, Eq. (B4) reduces to $\langle R_g^2 \rangle = b^2 N/6$, as expected for a Gaussian chain³⁸ and $\langle R_g^2 \rangle = (bN)^2/12 = L^2/12$ for a thin, rigid rod of length L (i.e., in the limit of $\nu = 1$).

APPENDIX C: SCATTERING FACTORS FOR A POLYMER CHAIN WITH EXCLUDED VOLUME

In this section, we derive expressions for the form factor $P(Q)$, form factor amplitude $F(Q)$, and the correlation between the chain ends $E(Q)$ for an isolated polymer chain with excluded volume. These expressions can be used to create scattering models for more complex systems such as block copolymers, polymer micelles, and polymer-grafted nanoparticles as described above in the main text. A graphical representation of the three functions is shown in Fig. 8.

1. Chain end correlations

The derivation of the scattering factors for a polymer chain assumes that regardless of the conformation of the chain (i.e., the value of the Flory exponent), the probability of two monomers i and j , which are $n = |i - j|$ monomers apart from each other, being separated by a distance r_{ij} is given by a Gaussian probability distribution,³⁸

$$P_{3D}(n, r_{ij}) = \left(\frac{3}{2\pi n b^2} \right)^{3/2} \exp\left(-\frac{3r_{ij}^2}{2n b^2} \right) \quad (C1)$$

02 March 2025 18:16:14

such that in a reciprocal space, the average value of the function is

$$\begin{aligned} \langle \exp(-Q^2 r_{ij}^2) \rangle &= \int \exp(-Qr_{ij}^2) P_{3d}(n, r_{ij}) dr_{ij} \\ &= \exp\left(-\frac{Q^2 \langle r_{ij}^2 \rangle}{6}\right), \end{aligned} \tag{C2}$$

where $\langle r_{ij}^2 \rangle$ is given by Eq. (B1). Note that although Eqs. (C1) and (C2) are, strictly speaking, only valid for $\nu = 1/2$, many experimental studies have used the result of Eq. (C2) to study polymer conformation for $\nu \neq 1/2$ with satisfactory results. With this caveat in mind, the correlation between chain ends represents the Fourier transform of the average value of r_{0N}^2 , which is simply the end-to-end distance of the polymer chain,

$$E(Q) \equiv \langle \exp(-Q^2 \langle r_{0N}^2 \rangle) \rangle = \exp(-Q^2 R_g^2). \tag{C3}$$

2. Form factor amplitude

The form factor amplitude is defined as $\langle \exp(-Q^2 r_{0j}^2) \rangle$, as illustrated in Fig. 8. Under the same assumptions outlined above for obtaining $E(Q)$ with $\nu \neq 1/2$, $F(Q)$ can be calculated as

$$\begin{aligned} F(Q) \equiv \langle \exp(-Q^2 r_{0j}^2) \rangle &= \frac{1}{N} \int_0^N \exp\left[-\frac{Q^2 b^2 (w-0)^{2\nu}}{6}\right] dw \\ &= \int_0^1 \exp\left[-\frac{Q^2 b^2 N^{2\nu} w^{2\nu}}{6}\right] dw', \end{aligned} \tag{C4}$$

where $w' = w/N$. Eq. (C4) can be solved analytically in the limit of $\nu = 1/2$ (Gaussian chain) to obtain

$$F(Q) = \frac{1 - \exp(-Q^2 R_g^2)}{Q^2 R_g^2}. \tag{C5}$$

However, for $\nu \neq 1/2$, there is no analytical solution to the integral. Instead, Eq. (C4) can be recast into the form

$$F(Q) = \frac{1}{2\nu U^{1/2\nu}} \int_0^U t^{(1/2\nu-1)} \exp(-t) dt \tag{C6}$$

by making the substitution $t = U w'^{2\nu}$, where $U = Q^2 b^2 N^{2\nu} / 6$. The form factor amplitude can then be expressed in terms of the lower incomplete gamma function

$$F(Q) = \frac{1}{2\nu U^{1/2\nu}} \gamma\left(\frac{1}{2\nu}, U\right), \tag{C7}$$

where the lower incomplete gamma function is defined as

$$\gamma(d, x) = \int_0^x t^{d-1} \exp(-t) dt. \tag{C8}$$

3. Form factor

The form factor for a polymer chain is defined as

$$\begin{aligned} P(Q) &\equiv \langle \exp(-Q^2 r_{ij}^2) \rangle \\ &= \frac{2}{N^2} \int_0^N du \int_u^N \exp\left[-\frac{Q^2 b^2 (w-u)^{2\nu}}{6}\right] dw \end{aligned} \tag{C9}$$

$$= 2 \int_0^1 du' \int_{u'}^1 \exp\left[-\frac{Q^2 b^2 (w'-u')^{2\nu}}{6}\right] dw', \tag{C10}$$

where $w' = w/N$ and $u' = u/N$. In the limit of $\nu = 1/2$, this expression can be evaluated analytically to obtain the form factor for a Gaussian chain (i.e., the Debye function),

$$P(Q) = \frac{2}{(Q^2 R_g^2)^2} \left[\exp(-Q^2 R_g^2) + Q^2 R_g^2 - 1 \right]. \tag{C11}$$

However, as with Eq. (C4), for $\nu \neq 1/2$, this expression cannot be evaluated analytically, and the form factor is given in terms of a difference of incomplete gamma functions.

To arrive at an expression for $P(Q)$, Eq. (C10) is evaluated in two steps. The inner integral is evaluated by first making the substitution $t = U(w' - u')^{2\nu}$ leaving

$$P(Q) = \frac{1}{\nu U^{1/2\nu}} \int_0^1 du' \int_0^{U(1-u')^{2\nu}} t^{(1/2\nu-1)} \exp(-t) dt \tag{C12}$$

$$= \frac{1}{\nu U^{1/2\nu}} \int_0^1 \gamma\left(\frac{1}{2\nu}, U(1-u')^{2\nu}\right) du' \tag{C13}$$

$$= \frac{1}{\nu U^{1/2\nu}} \int_0^U x^{(1/2\nu-1)} \gamma\left(\frac{1}{2\nu}, x\right) dx, \tag{C14}$$

where $x = U(1-u')^{2\nu}$. The final form factor is obtained using the identity

$$\int x^{b-1} \gamma(s, x) dx = \frac{1}{b} [x^b \gamma(s, x) - \gamma(s+b, x)] \tag{C15}$$

to yield

$$P(Q) = \frac{1}{\nu U^{1/2\nu}} \gamma\left(\frac{1}{2\nu}, U\right) - \frac{1}{\nu U^{1/2\nu}} \gamma\left(\frac{1}{\nu}, U\right). \tag{C16}$$

Note that Eq. (C16) also assumes that Eq. (C2) holds for $\nu \neq 1/2$. Furthermore, it has been noted that this expression does not reproduce the correct behavior of a thin rod with $\nu = 1$, and an alternative form factor must be used in that case. Comparing Eqs. (C5)–(C7) for the form factor amplitude to the form factors in Eqs. (C11)–(C16) confirms that for polymer chains, $P(Q) \neq |F(Q)|^2$.

02 March 2025 18:16:14

DATA AVAILABILITY

Data sharing is not applicable to this article as no new data were created or analyzed in this study.

REFERENCES

- ¹S. K. Kumar, N. Jouault, B. Benicewicz, and T. Neely, "Nanocomposites with polymer grafted nanoparticles," *Macromolecules* **46**, 3199–3214 (2013).
- ²M. J. A. Hore and R. J. Composto, "Functional polymer nanocomposites enhanced by nanorods," *Macromolecules* **47**, 875–887 (2014).
- ³J. Adelsberger, A. Kulkarni, A. Jain, W. Wang, A. M. Bivigou-Koumba, P. Busch, V. Pipich, O. Holderer, T. Hellweg, A. Laschewsky *et al.*, "Thermoresponsive PS-*b*-PNIPAM-*b*-PS micelles: Aggregation behavior, segmental dynamics, and thermal response," *Macromolecules* **43**, 2490–2501 (2010).
- ⁴A. S. Hoffman, "Applications of thermally reversible polymers and hydrogels in therapeutics and diagnostics," *J. Control. Release* **6**, 297–305 (1987).
- ⁵H. Feil, Y. H. Bae, J. Feijen, and S. W. Kim, "Molecular separation by thermosensitive hydrogel membranes," *J. Memb. Sci.* **64**, 283–294 (1991).
- ⁶Y. S. Park, Y. Ito, and Y. Imanishi, "Permeation control through porous membranes immobilized with thermosensitive polymer," *Langmuir* **14**, 910–914 (1998).
- ⁷A. Nykänen, M. Nuopponen, A. Laukkanen, S.-P. Hirvonen, M. Rytelä, O. Turunen, H. Tenhu, R. Mezzenga, O. Ikkala, and J. Ruokolainen, "Phase behavior and temperature-responsive molecular filters based on self-assembly of polystyrene-block-poly (*N*-isopropylacrylamide)-block-polystyrene," *Macromolecules* **40**, 5827–5834 (2007).
- ⁸G. Polymeropoulos, G. Zapsas, K. Ntetsikas, P. Bilalis, Y. Gnanou, and N. Hadjichristidis, "50th anniversary perspective: Polymers with complex architectures," *Macromolecules* **50**, 1253–1290 (2017).
- ⁹Z.-G. Wang, "50th anniversary perspective: Polymer conformation—A pedagogical review," *Macromolecules* **50**, 9073–9114 (2017).
- ¹⁰T. P. Lodge and P. C. Hiemenz, *Polymer Chemistry*, 3rd ed. (CRC Press, 2020).
- ¹¹A. Garcia-Rejon and C. Alvarez, "Mechanical and flow properties of high-density polyethylene/low-density polyethylene blends," *Polym. Eng. Sci.* **27**, 640–646 (1987).
- ¹²J. Lyngso, N. Al-Manasir, M. A. Behrens, K. Zhu, A.-L. Kjøniksen, B. Nyström, and J. S. Pedersen, "Small-angle x-ray scattering studies of thermoresponsive poly(*N*-isopropylacrylamide) star polymers in water," *Macromolecules* **48**, 2235–2243 (2015).
- ¹³L. Willner, O. Jucknischke, D. Richter, J. Roovers, L.-L. Zhou, P. Toporowski, L. Fetters, J. Huang, M. Lin, and N. Hadjichristidis, "Structural investigation of star polymers in solution by small-angle neutron scattering," *Macromolecules* **27**, 3821–3829 (1994).
- ¹⁴A. Chremos and J. F. Douglas, "Communication: When does a branched polymer become a particle?," *J. Chem. Phys.* **143**, 111104 (2015).
- ¹⁵C. M. Bates and F. S. Bates, "50th anniversary perspective: Block polymers—Pure potential," *Macromolecules* **50**, 3–22 (2017).
- ¹⁶U. Tritschler, S. Pearce, J. Gwyther, G. R. Whittell, and I. Manners, "50th anniversary perspective: Functional nanoparticles from the solution self-assembly of block copolymers," *Macromolecules* **50**, 3439–3463 (2017).
- ¹⁷X. Zhou, X. Ye, and G. Zhang, "Thermoresponsive triblock copolymer aggregates investigated by laser light scattering," *J. Phys. Chem. B* **111**, 5111–5115 (2007).
- ¹⁸A. Papagiannopoulos, J. Zhao, G. Zhang, S. Pispas, and A. Radulescu, "Thermoresponsive aggregation of PS-PNIPAM-PS triblock copolymer: A combined study of light scattering and small angle neutron scattering," *Eur. Polym. J.* **56**, 59–68 (2014).
- ¹⁹W. Wang, C. Gao, Y. Qu, Z. Song, and W. Zhang, "In situ synthesis of thermoresponsive polystyrene-*b*-poly (*N*-isopropylacrylamide)-*b*-polystyrene nanospheres and comparative study of the looped and linear poly (*N*-isopropylacrylamide)s," *Macromolecules* **49**, 2772–2781 (2016).
- ²⁰W.-L. Chen, R. Cordero, H. Tran, and C. K. Ober, "50th anniversary perspective: Polymer brushes: Novel surfaces for future materials," *Macromolecules* **50**, 4089–4113 (2017).
- ²¹M. J. A. Hore, "Polymers on nanoparticles: Structure & dynamics," *Soft Matter* **15**, 1120–1134 (2019).
- ²²Y. Wei, X. Lang, and M. J. A. Hore, "A correspondence between the Flory–Rehner theory for microgels and the Daoud–Cotton model for polymer-grafted nanoparticles," *J. Appl. Phys.* **128**, 214701 (2020).
- ²³R. Ashkar, "Selective dynamics in polymeric materials: Insights from quasi-elastic neutron scattering spectroscopy," *J. Appl. Phys.* **127**, 151101 (2020).
- ²⁴J. Higgins and H. Benoit, *Polymers and Neutron Scattering* (Oxford University Press, 2002).
- ²⁵B. Hammouda, see https://www.ncnr.nist.gov/staff/hammouda/the_SANS_toolbox.pdf for "Probing Nanoscale Structures—The SANS Toolbox" (2020); accessed 28 January 2021.
- ²⁶L. Porcar, D. Pozzo, G. Langenbacher, J. Moyer, and P. D. Butler, "Rheo-small-angle neutron scattering at the National Institute of Standards and Technology Center for Neutron Research," *Rev. Sci. Instrum.* **82**, 083902 (2011).
- ²⁷E. H. Lehmann and W. Wagner, "Neutron imaging at PSI: A promising tool in materials science and technology," *Appl. Phys. A* **99**, 627–634 (2010).
- ²⁸I. A. Zaliznyak and J. M. Tranquada, "Neutron scattering and its application to strongly correlated systems," in *Strongly Correlated Systems* (Springer, 2015), pp. 205–235.
- ²⁹R. Pynn, "Neutron scattering: A primer," *Los Alamos Sci.* **19**, 1–31 (1990).
- ³⁰E. Fermi, "Sul moto dei neutroni nelle sostanze idrogenate," *Ric. Sci.* **7**, 13–52 (1936).
- ³¹F. S. Varley, "Neutron scattering lengths and cross section," *Neutron News* **3**, 29–37 (1992).
- ³²M. Shibayama, "Small-angle neutron scattering on polymer gels: Phase behavior, inhomogeneities and deformation mechanisms," *Polym. J.* **43**, 18 (2011).
- ³³J. Lu, F. Bates, and T. Lodge, "Chain exchange in binary copolymer micelles at equilibrium: Confirmation of the independent chain hypothesis," *ACS Macro Lett.* **2**, 451–455 (2013).
- ³⁴I. Kugler, E. W. Fischer, M. Peuscher, and C. D. Eisenbach, "Small angle neutron scattering studies of poly (ethylene oxide) in the melt," *Die Makromol. Chem.: Macromol. Chem. Phys.* **184**, 2325–2334 (1983).
- ³⁵Y. Wei, Y. Xu, A. Faraone, and M. J. Hore, "Local structure and relaxation dynamics in the brush of polymer-grafted silica nanoparticles," *ACS Macro Lett.* **7**, 699–704 (2018).
- ³⁶R.-J. Roe and R. Roe, *Methods of X-ray and Neutron Scattering in Polymer Science* (Oxford University Press, New York, 2000), Vol. 739.
- ³⁷J. M. Carpenter and C.-K. Loong, *Elements of Slow-Neutron Scattering* (Cambridge University Press, 2015).
- ³⁸M. Rubinstein, R. H. Colby *et al.*, *Polymer Physics* (Oxford University Press, New York, 2003).
- ³⁹A. Guinier, G. Fournet, and K. L. Yudowitch, *Small-Angle Scattering of X-rays* (John Wiley & Sons, Inc., 1955).
- ⁴⁰O. Kratky, "X-ray small angle scattering with substances of biological interest in diluted solutions," *Prog. Biophys. Mol. Biol.* **13**, 105–173 (1963).
- ⁴¹O. Glatter and O. Kratky, *Small Angle X-Ray Scattering* (Academic Press, 1982).
- ⁴²L. Feigin, D. I. Svergun *et al.*, *Structure Analysis by Small-Angle X-Ray and Neutron Scattering* (Springer, 1987), Vol. 1.
- ⁴³R. P. Hjelm, Jr., P. Thiyagarajan, and H. Alkan-Onyuksel, "Organization of phosphatidylcholine and bile salt in rodlike mixed micelles," *J. Phys. Chem.* **96**, 8653–8661 (1992).
- ⁴⁴T. E. Gartner III, F. M. Haque, A. M. Gomi, S. M. Grayson, M. J. Hore, and A. Jayaraman, "Scaling exponent and effective interactions in linear and cyclic

- polymer solutions: Theory, simulations, and experiments,” *Macromolecules* **52**, 4579–4589 (2019).
- ⁴⁵P. Debye, “Molecular-weight determination by light scattering,” *J. Phys. Chem.* **51**, 18–32 (1947).
- ⁴⁶I. Grillo, “Small-angle neutron scattering and applications in soft condensed matter,” in *Soft Matter Characterization*, edited by R. Borsali and R. Pecora (Springer, 2008), Chap. 13, pp. 723–782.
- ⁴⁷C. D. Putnam, “Guinier peak analysis for visual and automated inspection of small-angle x-ray scattering data,” *J. Appl. Crystallogr.* **49**, 1412–1419 (2016).
- ⁴⁸A. Husain, J. Reddy, D. Bisht, and M. Sajid, “Fractal dimension of coastline of Australia,” *Sci. Rep.* **11**, 1 (2021).
- ⁴⁹G. Porod, “Die röntgenkleinwinkelstreuung von dichtgepackten kolloiden systemen,” *Kolloid-Zeitschrift* **124**, 83–114 (1951).
- ⁵⁰B. Hammouda, “A new Guinier–Porod model,” *J. Appl. Crystallogr.* **43**, 716–719 (2010).
- ⁵¹B. Hammouda, “Form factors for branched polymers with excluded volume,” *J. Res. Natl. Inst. Stand. Technol.* **121**, 139–164 (2016).
- ⁵²G. Beaucage, “Approximations leading to a unified exponential/power-law approach to small-angle scattering,” *J. Appl. Crystallogr.* **28**, 717–728 (1995).
- ⁵³L. M. Yablon, S. N. Sanders, H. Li, K. R. Parenti, E. Kumarasamy, K. J. Fallon, M. J. A. Hore, A. Cacciuto, M. Y. Sfeir, and L. M. Campos, “Persistent multiexcitons from polymers with pendent pentacenes,” *J. Am. Chem. Soc.* **141**, 9564–9569 (2019).
- ⁵⁴P. W. Lee, S. A. Isarov, J. D. Wallat, S. K. Molugu, S. Shukla, J. E. P. Sun, J. Zhang, Y. Zheng, M. Lucius Dougherty, D. Konkolewicz, P. L. Stewart, N. F. Steinmetz, M. J. A. Hore, and J. K. Pokorski, “Polymer structure and conformation alter the antigenicity of virus-like particle–polymer conjugates,” *J. Am. Chem. Soc.* **139**, 3312–3315 (2017).
- ⁵⁵G. Beaucage, “Small-angle scattering from polymeric mass fractals of arbitrary mass-fractal dimension,” *J. Appl. Crystallogr.* **29**, 134–146 (1996).
- ⁵⁶B. Hammouda, “Analysis of the Beaucage model,” *J. Appl. Crystallogr.* **43**, 1474–1478 (2010).
- ⁵⁷B. Hammouda and M.-H. Kim, “The empirical core-chain model,” *J. Mol. Liq.* **247** 434–440 (2017).
- ⁵⁸P. Debye and A. Bueche, “Scattering by an inhomogeneous solid,” *J. Appl. Phys.* **20**, 518–525 (1949).
- ⁵⁹P. Debye, H. Anderson, Jr., and H. Brumberger, “Scattering by an inhomogeneous solid. II. The correlation function and its application,” *J. Appl. Phys.* **28**, 679–683 (1957).
- ⁶⁰P.-G. De Gennes *Scaling Concepts in Polymer Physics* (Cornell University Press, 1979).
- ⁶¹B. Hammouda, D. L. Ho, and S. Kline, “Insight into clustering in poly(ethylene oxide) solutions,” *Macromolecules* **37**, 6932–6937 (2004).
- ⁶²P. Debye, “Zerstreuung von röntgenstrahlen,” *Ann. Phys.* **351**, 809–823 (1915).
- ⁶³P. J. Flory, *Principles of Polymer Chemistry* (Cornell University Press, 1953).
- ⁶⁴B. Hammouda, “SANS from homogeneous polymer mixtures: A unified overview,” in *Polymer Characteristics* (Springer, 1993), pp. 87–133.
- ⁶⁵N. Hadjichristidis, “Synthesis of miktoarm star (μ -star) polymers,” *J. Polym. Sci. Part A: Polym. Chem.* **37**, 857–871 (1999).
- ⁶⁶H. Benoit, “On the effect of branching and polydispersity on the angular distribution of the light scattered by Gaussian coils,” *J. Polym. Sci.* **11**, 507–510 (1953).
- ⁶⁷X. Lang, W. R. Lenart, J. E. Sun, B. Hammouda, and M. J. Hore, “Interaction and conformation of aqueous poly (N -isopropylacrylamide) (PNIPAM) star polymers below the LCST,” *Macromolecules* **50**, 2145–2154 (2017).
- ⁶⁸J. L. Alessandrini and M. A. Carignano, “Static scattering function for a regular star-branched polymer,” *Macromolecules* **25**, 1157–1163 (1992).
- ⁶⁹J. D. Halverson, G. S. Grest, A. Y. Grosberg, and K. Kremer, “Rheology of ring polymer melts: From linear contaminants to ring-linear blends,” *Phys. Rev. Lett.* **108**, 038301 (2012).
- ⁷⁰N. Nasongkla, B. Chen, N. Macaraeg, M. E. Fox, J. M. Fréchet, and F. C. Szoka, “Dependence of pharmacokinetics and biodistribution on polymer architecture: Effect of cyclic versus linear polymers,” *J. Am. Chem. Soc.* **131**, 3842–3843 (2009).
- ⁷¹Q. Wu, P. M. Rauscher, X. Lang, R. J. Wojtecki, J. J. de Pablo, M. J. A. Hore, and S. J. Rowan, “Poly[n]catenanes: Synthesis of molecular interlocked chains,” *Science* **358**, 1434–1439 (2017).
- ⁷²A. Takano, Y. Ohta, K. Masuoka, K. Matsubara, T. Nakano, A. Hieno, M. Itakura, K. Takahashi, S. Kinugasa, D. Kawaguchi, Y. Takahashi, and Y. Matsushita, “Radii of gyration of ring-shaped polystyrenes with high purity in dilute solutions,” *Macromolecules* **45**, 369–373 (2012).
- ⁷³T. Iwamoto, Y. Doi, K. Kinoshita, A. Takano, Y. Takahashi, E. Kim, T.-H. Kim, S.-I. Takata, M. Nagao, and Y. Matsushita, “Conformations of ring polystyrenes in semidilute solutions and in linear polymer matrices studied by SANS,” *Macromolecules* **51**, 6836–6847 (2018).
- ⁷⁴B. Hammouda, “Structure factors for regular polymer gels and networks,” *J. Chem. Phys.* **99**, 9182–9187 (1993).
- ⁷⁵S. L. Pesek, Q. Xiang, B. Hammouda, and R. Verduzco, “Small-angle neutron scattering analysis of bottlebrush backbone and side chain flexibility,” *J. Polym. Sci. Part B: Polym. Phys.* **55**, 104–111 (2017).
- ⁷⁶S. L. Pesek, X. Li, B. Hammouda, K. Hong, and R. Verduzco, “Small-angle neutron scattering analysis of bottlebrush polymers prepared via grafting-through polymerization,” *Macromolecules* **46**, 6998–7005 (2013).
- ⁷⁷S. Rathgeber, T. Pakula, A. Wilk, K. Matyjaszewski, and K. L. Beers, “On the shape of bottle-brush macromolecules: Systematic variation of architectural parameters,” *J. Chem. Phys.* **122**, 124904 (2005).
- ⁷⁸J. S. Pedersen and M. C. Gerstenberg, “Scattering form factor of block copolymer micelles,” *Macromolecules* **29**, 1363–1365 (1996).
- ⁷⁹J. S. Pedersen, “Analysis of small-angle scattering data from colloids and polymer solutions: Modeling and least-squares fitting,” *Adv. Colloid Interface Sci.* **70**, 171–210 (1997).
- ⁸⁰M. J. Hore, J. Ford, K. Ohno, R. J. Composto, and B. Hammouda, “Direct measurements of polymer brush conformation using small-angle neutron scattering (SANS) from highly grafted iron oxide nanoparticles in homopolymer melts,” *Macromolecules* **46**, 9341–9348 (2013).
- ⁸¹A. V. Zhukhovitskiy, J. Zhao, M. Zhong, E. G. Keeler, E. A. Alt, P. Teichen, R. G. Griffin, M. J. A. Hore, A. P. Willard, and J. A. Johnson, “Polymer structure dependent hierarchy in polymoc gels,” *Macromolecules* **49**, 6896–6902 (2016).
- ⁸²K. Larson-Smith, A. Jackson, and D. C. Pozzo, “Small angle scattering model for pickering emulsions and raspberry particles,” *J. Colloid Interface Sci.* **343**, 36–41 (2010).
- ⁸³X. Lang, A. D. Patrick, B. Hammouda, and M. J. Hore, “Chain terminal group leads to distinct thermoresponsive behaviors of linear PNIPAM and polymer analogs,” *Polymer* **145**, 137–147 (2018).
- ⁸⁴D. Schwahn, “Critical to mean field crossover in polymer blends,” in *Phase Behaviour of Polymer Blends*, edited by K. F. Freed (Springer, 2005), pp. 1–61.
- ⁸⁵M. J. A. Hore, B. Hammouda, Y. Li, and H. Cheng, “Co-nonsolvency of poly (n -isopropylacrylamide) in deuterated water/ethanol mixtures,” *Macromolecules* **46**, 7894–7901 (2013).
- ⁸⁶A. Z. Akcasu, R. Klein, and B. Hammouda, “Dynamics of multicomponent polymer mixtures via the random phase approximation including hydrodynamic interactions,” *Macromolecules* **26**, 4136–4143 (1993).
- ⁸⁷M. Benmouna and B. Hammouda, “The zero average contrast condition: Theoretical predictions and experimental examples,” *Prog. Polym. Sci.* **22**, 49–92 (1997).

- ⁸⁸B. Hammouda, D. Jia, and H. Cheng, "Single-chain conformation for interacting poly(N-isopropylacrylamide) in aqueous solution," *Open Access J. Sci. Technol.* **3**, 101152 (2015).
- ⁸⁹M. Benmouna, E. W. Fischer, B. Ewen, and M. Duval, "On the measurement of the X-parameter under the zero average contrast condition," *J. Polym. Sci. Part B: Polym. Phys.* **30**, 1157–1164 (1992).
- ⁹⁰N. Jouault, M. K. Crawford, C. Chi, R. J. Smalley, B. Wood, J. Jestin, Y. B. Melnichenko, L. He, W. E. Guise, and S. K. Kumar, "Polymer chain behavior in polymer nanocomposites with attractive interactions," *ACS Macro Lett.* **5**, 523–527 (2016).
- ⁹¹R. Andrae, T. Schulze-Hartung, and P. Melchior, "Dos and don'ts of reduced chi-squared," *arXiv:1012.3754* (2010).
- ⁹²M. M. Noack, K. G. Yager, M. Fukuto, G. S. Doerk, R. Li, and J. A. Sethian, "A Kriging-based approach to autonomous experimentation with applications to x-ray scattering," *Sci. Rep.* **9**, 11809 (2019).
- ⁹³D. J. Beltran-Villegas, M. G. Wessels, J. Y. Lee, Y. Song, K. L. Wooley, D. J. Pochan, and A. Jayaraman, "Computational reverse-engineering analysis for scattering experiments on amphiphilic block polymer solutions," *J. Am. Chem. Soc.* **141**, 14916–14930 (2019).